LA-8874-PR

Progress Report

Applied Nuclear Data Research and Development

January 1—March 31, 1981

University of California

LOS ALAMOS SCIENTIFIC LABORATORY

Post Office Box 1663 Los Alamos, New Mexico 87545

LA-8874-PR
Progress Report

UC-34c
Issued: July 1981

Applied Nuclear Data Research and Development

January 1—March 31, 1981

Compiled by

C. I. Baxman
P. G. Young

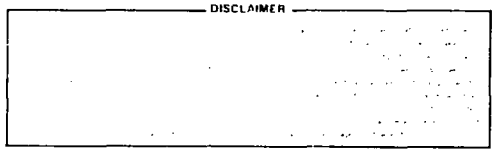

TABLE OF CONTENTS

APPLIED NUCLEAR DATA RESEARCH AND DEVELOPMENT
QUARTERLY PROGRESS REPORT
January 1 - March 31, 1981

Compiled by

C. I. Baxman and P. G. Young

ABSTRACT

This progress report describes the activities of the Los Alamos Nuclear Data Group for January 1 through March 31, 1981. The topical content is summarized in the Table of Contents.

I. THEORY AND EVALUATION OF NUCLEAR CROSS SECTIONS

A. Peripheral Effects in R-Matrix Theory (G. M. Hale)

Peripheral effects due to the exponential tails of bound-state wavefunctions extending beyond the range of the nuclear forces are believed to be important in a number of few-body reactions. The so-called "particle exchange" pole comes naturally out of the plane-wave Born approximation to the T matrix for single-particle-transfer descriptions of two-body reactions, but the corresponding term has not been identified in R-matrix theory.

We have shown in the simple case of two colinear particles, which interact via finite-ranged potentials with an impenetrable center of force, that the particle-exchange term also arises quite naturally in R-matrix theory if the finite extent of the internal region is properly taken into account when defining the boundary-condition operator that makes the internal system Hamiltonian Hermitian and when matching to the Lippmann-Schwinger equations on the surface bounding the internal region. The term appears as a simple pole located at the (negative) sum of the binding energies of the two particles with a residue equal to the product of the reduced-width amplitudes for the bound-state wave functions. These parameters are generally known for the light nuclei, but they can be determined from data fitting as are the R-matrix parameters themselves.

The generalization of this theory to a more realistic three-dimensional particle-exchange model is somewhat complex, but it will allow peripheral effects to be incorporated in a unitary fashion with both the short-range (nuclear) forces and the longer range Coulomb/angular momentum barrier. It is expected to enhance the ability of R-matrix theory to describe reactions in light nuclei and to better explain the origin of certain nonresonant features in the data.

B. Coulomb Corrections in Light Nuclei [G. M. Hale and H. Zankel (U. Graz)]

The work described in last quarter's report[1] on Coulomb differences between the nucleon-deuteron reactions has been combined with similar calculations for nucleon-nucleon scattering in an article submitted to Physical Review.

C. New R-Matrix Analysis of Reactions in the ^{7}Li System (G. M. Hale and D. C. Dodder)

Precise new experimental data for t-α elastic scattering and for the n-^{6}Li reactions have recently become available. Most of these measurements are quite consistent for energies corresponding to $E_n < 2.5$ MeV with the R-matrix analysis we had used earlier to provide n-^{6}Li cross sections, including the ^{6}Li(n,t) standard cross sections, for ENDF/B-V. However, the new data extend to higher energies than the range of the previous analysis.

A new R-matrix analysis of reactions in the ^{7}Li system has been started from the earlier results, including the new data up to higher energies (E_n = 4 MeV, E_t = 14.4 MeV). The goals of this new analysis are to provide n -^{6}Li cross sections for ENDF/B-VI, in particular, ^{6}Li(n,t) cross sections reliable enough to be used as a standard up to a few MeV, and to investigate the level structure of ^{7}Li at excitation energies above 10 MeV, where evidence[2,3] for a $1/2^-$ level apparently exists in some of the new data.

D. Variance-Covariance Analysis of n + ^{7}Li Reactions (P. G. Young)

An evaluation of n + ^{7}Li nuclear data for neutron energies between 0.1 and 20 MeV using variance-covariance techniques is in progress. The analysis utilizes the GLUCS[4] code system to perform variance-covariance analyses of each of the major cross-section types for which experimental data exist. That is, GLUCS is used to determine evaluated cross sections and covariances for each reaction type from inputted experimental cross sections and covariances. The results of

the GLUCS analysis are then combined using the ALVIN[5] code under the constraint that all partial reactions sum to the total cross section, with full account being taken of all covariances.

The four primary reactions that are included in the analysis are the total cross section, the combined elastic plus (n,n_1') to the 0.476-MeV first excited ^{7}Li state, the (n,n't), and the combined (n,2n) plus all other reactions [mainly the (n,d)]. The sum of the latter three reactions equals the total cross section. The elastic plus (n,n_1') was treated together because most of the available elastic scattering measurements do not resolve the first excited state. A separate GLUCS analysis was carried out for the large mass of ^{7}Li$(n,n'\gamma)$ data that is available, which corresponds to the (n,n_1') cross section. These results were used to separate the (n,n_1') cross section from the combined elastic plus (n,n_1') cross section determined in the main GLUCS/ALVIN analysis. Similarly, the combined (n,2n) plus (n,d) results from the GLUCS/ALVIN analysis were split into the constituent (n,2n), (n,2nd), and (n,d) reactions using ENDF/B-V data.

To perform this analysis, it was necessary to obtain covariance matrices for each experimental data measurement. In some instances, sufficient information was available to directly infer the correlations in the experimental data. In most cases, however, it was necessary to make simple generic assumptions regarding the correlations present in different types of measurements. For example, modern total cross-section measurements were generally assumed to have a normalization error of the order of $\approx 0.5\%$ due to sample thickness and composition uncertainty. Greater normalization uncertainty was assumed for older measurements. The final GLUCS/ALVIN cross sections were not found to be highly sensitive to the exact assumptions made, although it was observed that significant overestimates of correlations could distort results, especially in energy regions where measured data are scarce.

The GLUCS code system permits considerable flexibility in that experimental data and evaluated results need not lie on the same energy grid, and the covariance grid can be a subset of the evaluation energy grid. It is difficult, however, to unambiguously interpolate covariances, and the effect of introducing an experimental datum between two evaluated grid points is to introduce a correlation between the evaluated data at the two grid points that has little to do with actual correlations in the measurement. To avoid such difficulties, a common energy grid was used throughout this work for all experimental and evaluated data, including covariances. A total of 49 energy grid points was used for the neutron energy range 0.1–20 MeV.

Several utility codes were developed during this analysis. The code AVRAGE was written to average a given number of experimental data points selected for a given reference from an ECSIL[6] card-image experimental data file, with the option of combining a normalization error with the statistical errors in the input experimental data. A second code, COVEXP, was developed to interpolate/extrapolate the experimental data onto the analysis energy grid, using the input evaluated data for the GLUCS analysis as an interpolation guide. In addition, COVEXP prepares the input experimental data file for the GLUCS analysis, with the option of either direct relative covariance input or use of simple, compact (but general) algorithms for constructing the covariances. A third code, ALVINP, was written to convert the GLUCS output cross sections and covariances from the total and partial reaction cross-section analyses into the proper input file for the ALVIN code. Finally, a code called ALVOUT was developed to assemble the results from the ALVIN analysis into both human-readable forms and ENDF/B decks. At present, ALVOUT only creates an MF=3 type ENDF deck, but it will be expanded soon to output the necessary MF=33 decks.

All available experimental data for which error estimates were possible were used in the GLUCS analyses. A simple error doubling procedure was followed for measurements that differed by more than two standard deviations from trial results from GLUCS. Such a procedure was necessary for some 12 experiments out of the 56 used in the work. A total of 4200 data points were included in the analysis.

The only experimental data available in the energy range 15-20 MeV are the total and $(n,n'\gamma)$ cross sections. Therefore, in order to permit an accurate separation of the partial cross sections at these energies, an optical-model analysis was performed covering the energy range 10-20 MeV. The elastic angular distribution measurements of Hogue et al.[7] at 10, 12, and 14 MeV and the evaluated total cross section from 10-20 MeV were fit using the SCATOPT code.[8] The resulting spherical optical parameters are given in Table I. These results were used to compute elastic cross sections from 16-20 MeV for inclusion in the GLUCS analysis.

The adjustment factors from the ALVIN analysis, that is, the factors required to multiply the ALVIN input cross sections (output cross sections from the GLUCS analysis) in order to minimize the composite χ^2 of the entire cross section/covariance system are shown in Table II for the full analysis grid. As expected, the adjustment factors for the total cross section are nearly unity

TABLE I

SPHERICAL OPTICAL MODEL PARAMETERS FOR n + ^{7}Li INTERACTIONS WITH $10 \leq E_n \leq 20$ MeV

	r(fm)	a(fm)
V (MeV) = 42.94 - 0.35 E	1.206	0.718
W_{SD} (MeV) = 3.974 - 0.027 E	1.05	0.757
V_{SO} (MeV) = 5.500	1.15	0.57

because of the generally high accuracy of these measurements. The largest adjustments are seen for the elastic + (n,n_1') below the (n,nt) threshold and for the (n,2n) + (n,d) reaction. In both cases, the input experimental data are generally older and the errors larger. The adjustments for the elastic + (n,n_1') and for the (n,nt) reaction above the latter's threshold differ from unity by generally less that 5%, highlighting the consistency of the total and partial cross sections from the *GLUCS analysis*. An exception is the 0.70 adjustment factor for the (n,nt) reaction at 5.4 MeV. At this energy, however, the (n,nt) reaction is changing rapidly with energy, and the large adjustment probably indicates a slight inconsistency between the energy scales of the total and (n,nt) measurements.

The adjusted points from the ALVIN analysis for the total cross sections vary smoothly with energy and were used directly to generate the final evaluated data file. The (n,nt) results, however, are not as smooth because of the smaller and less consistent experimental data base that went into the analysis. It was therefore necessary to smooth the (n,nt) results for the final cross-section evaluation. The smoothed curve is compared to the ALVIN results (points with errors bars) in Fig. 1.

The final evaluated total and elastic + (n,n_1') cross sections from 2-16 MeV are compared to selected experiments and to ENDF/B-V in Fig. 2. Similarly, the evaluated ^{7}Li(n,nt) cross section is compared to the measurements used in the analysis and to ENDF/B-V in Fig. 3. It is readily seen from Figs. 2 and 3 that the major difference between these results and ENDF/B-V is a lowering of the (n,nt) cross section between 6-20 MeV and a corresponding increase in the

TABLE II

ADJUSTMENT FACTORS FOR n + ^{7}Li CROSS SECTIONS
DETERMINED IN ALVIN ANALYSIS

E (MeV)	F (total)	F (n,n + n,n'$_1$)	F (n,nt)	F (n, 2n + n,d)
0.10	0.9964	1.1411		
0.14	0.9996	1.1872		
0.18	0.9990	1.2698		
0.22	1.0087	0.8310		
0.24	0.9997	0.9713		
0.26	0.9989	1.1796		
0.28	0.9979	1.2221		
0.30	0.9970	1.0986		
0.34	1.0013	0.9834		
0.40	1.0001	0.9931		
0.50	1.0004	0.9620		
0.60	0.9998	1.0094		
0.75	1.0000	0.9870		
0.90	0.9996	1.0312		
1.00	0.9995	1.0713		
1.20	0.9985	1.0871		
1.40	0.9988	1.0564		
1.80	1.0003	1.0188		
2.20	0.9979	1.0628		
2.60	0.9997	1.0782	1.0000	
3.00	0.9993	1.0468	1.0055	
3.40	1.0006	0.9750	0.9214	
3.80	1.0002	0.9663	0.9917	
4.20	1.0004	0.9873	0.9148	
4.40	0.9999	0.9797	0.9997	
4.60	1.0002	0.9825	0.9952	
5.00	0.9996	0.9909	1.0044	
5.40	1.0012	0.9519	0.7040	
5.60	1.0000	0.9822	0.9976	
5.80	0.9984	1.0090	1.0594	
6.00	0.9994	1.0031	1.0410	
6.50	1.0008	0.9755	0.9241	
7.00	0.9995	1.0009	0.9995	
7.50	0.9980	1.0224	1.0460	
8.00	1.0004	0.9534	0.9871	1.0000
8.50	0.9999	1.0076	0.9985	1.0000
9.00	1.0000	0.9909	0.9943	0.9921
9.50	0.9998	0.9526	1.0044	0.9998
10.00	1.0008	0.9763	0.9542	0.8775
11.00	0.9998	0.9953	0.9928	1.0113
12.00	0.9994	1.0025	1.0161	1.3459
13.00	0.9996	0.9981	1.0055	1.1202
14.00	0.9984	1.0244	1.0078	1.0043
15.00	1.0000	1.0231	0.9987	0.4518
16.00	0.9997	1.0254	1.0368	1.0117
17.00	0.9997	1.0289	1.0341	1.0114
18.00	0.9997	1.0311	1.0239	1.0083
19.00	0.9996	1.0359	1.0617	1.0223
20.00	0.9996	1.0360	1.1093	1.0407

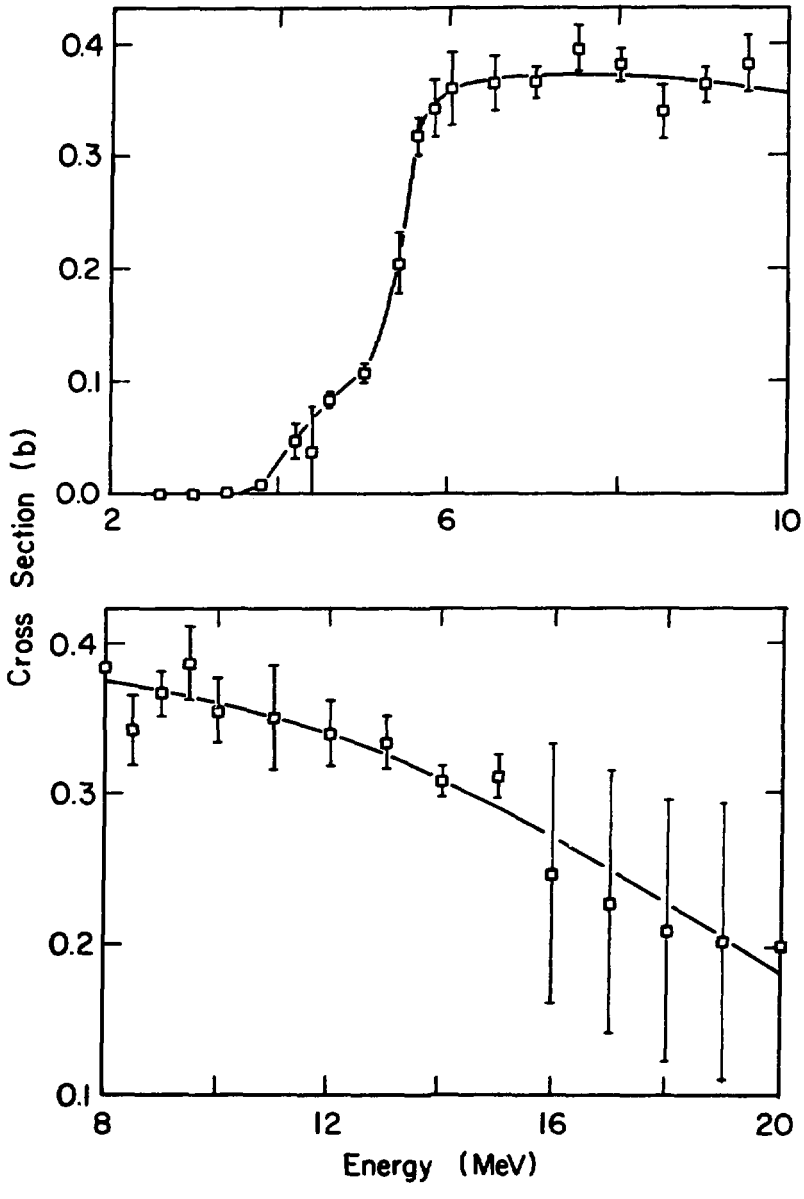

Fig. 1.
Comparison of smoothed evaluated ^{7}Li(n,nt) cross section with fitted cross sections and standard deviations from the GLUCS/ ALVIN analysis.

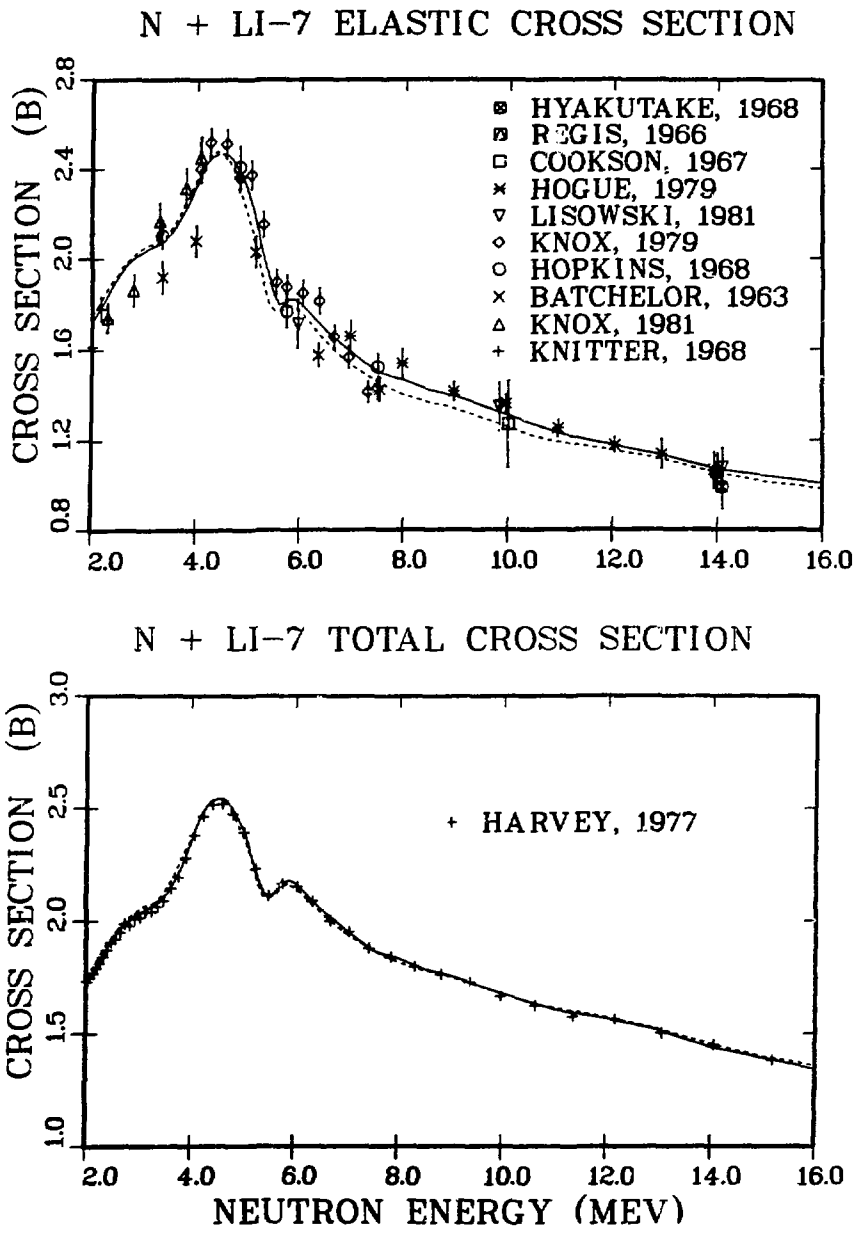

Fig. 2.
Evaluated and experimental n + ^{7}Li elastic plus (n,n') (upper half) and total (lower half) cross sections. The solid curve is the present result and the dashed curve is ENDF/B-V.

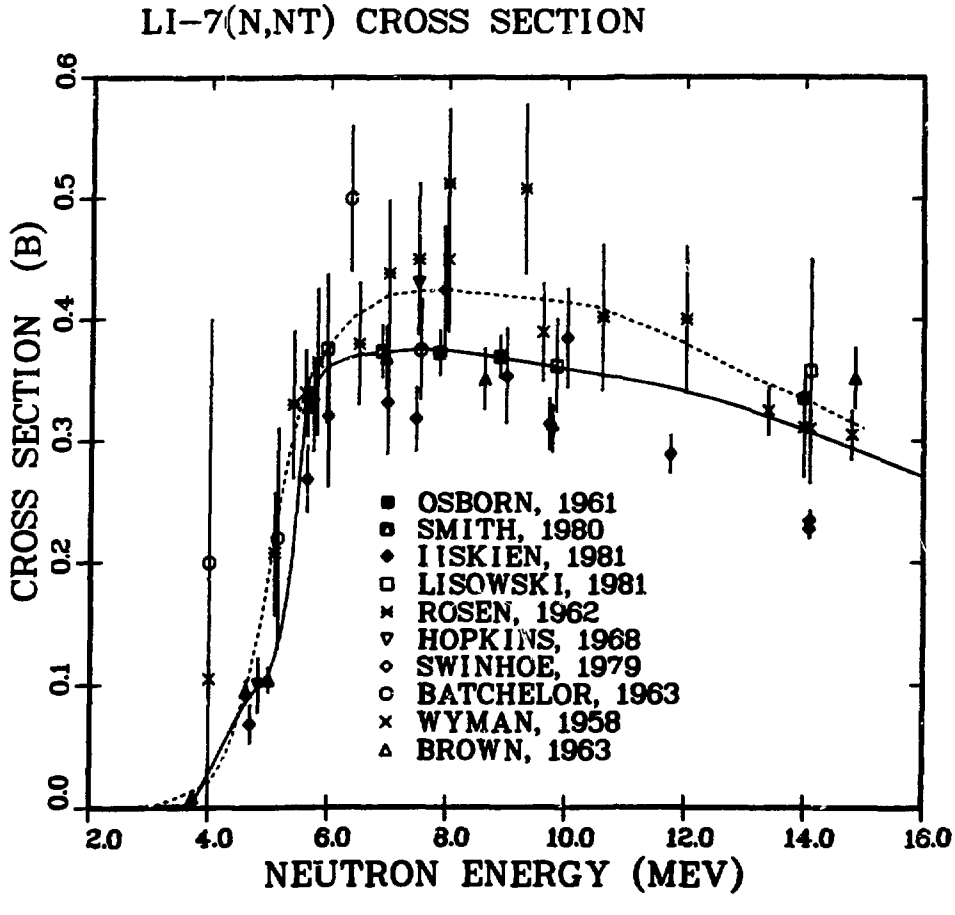

Fig. 3.
Evaluated and experimental ^{7}Li(n,nt) cross sections. The solid curve is the present result and the dashed curve is ENDF/B-V.

elastic plus (n,n_1') cross section. The (n,nt) cross section is in excellent agreement with the recent measurement by Smith et al.[9] between 7-9 MeV but is significantly higher than the Swinhoe[10] data from Harwell. The (n,nt) results are 15% lower than ENDF/B-V at 10 MeV and 9% lower at 14 MeV.

Other features of this new evaluation are a complete re-analysis of all elastic and inelastic angular distributions, a division of the (n,nt) cross section into a series of excitation energy bins that permit inclusion of accurate energy-angle correlations for emission neutrons, and complete covariance files for all cross-section data, including emission neutrons. Work on the last two items is still in progress.

E. Calculated Charged-Particle Emission in the Mass-90 Region (E. D. Arthur)

Neutron induced charged-particle emission, particularly that involving protons, constitutes a non-negligible portion of the total reaction cross section in the mass-90 region. Furthermore, our calculations for stable and unstable yttrium isotopes[11] showed that for target nuclei where the proton binding energy was significantly lower than the neutron's, large proton emission cross sections could be expected with major contributions arising from the (n,np) reaction. Such behavior is illustrated in Fig. 4. The calculated (n,np) cross sections are most sensitive to the sub-Coulomb barrier behavior of the proton transmission coefficients, the amount of gamma-ray competition included, and to the level density assumed for the second decaying compound system. New measurements performed by Haight et al.[12] at Livermore, in which charged-particle production spectra induced by 15-MeV neutrons on nuclei in this mass region were measured, provide an opportunity to test our previous calculations. Furthermore several of the target nuclei have a proton binding energy significantly lower than that of the neutron so that parameters can be verified under conditions similar to those occurring for the yttrium isotopes shown in Fig. 4.

Figure 5 compares our calculated spectra to data measured for ^{89}Y, ^{90}Zr, and ^{92}Mo. [The dashed lines indicate the sum of calculated (n,np + n,pn) contributions to the spectra that will be discussed later.] These nuclei have differences in proton and neutron binding energies that are 4.4, 3.6, and 5.2 MeV, respectively. The yttrium calculations shown in Fig. 5 were taken directly from our 1978 effort while the ^{90}Zr and ^{92}Mo theoretical calculations were made recently using updated proton optical parameters determined by Lagrange.[13] In

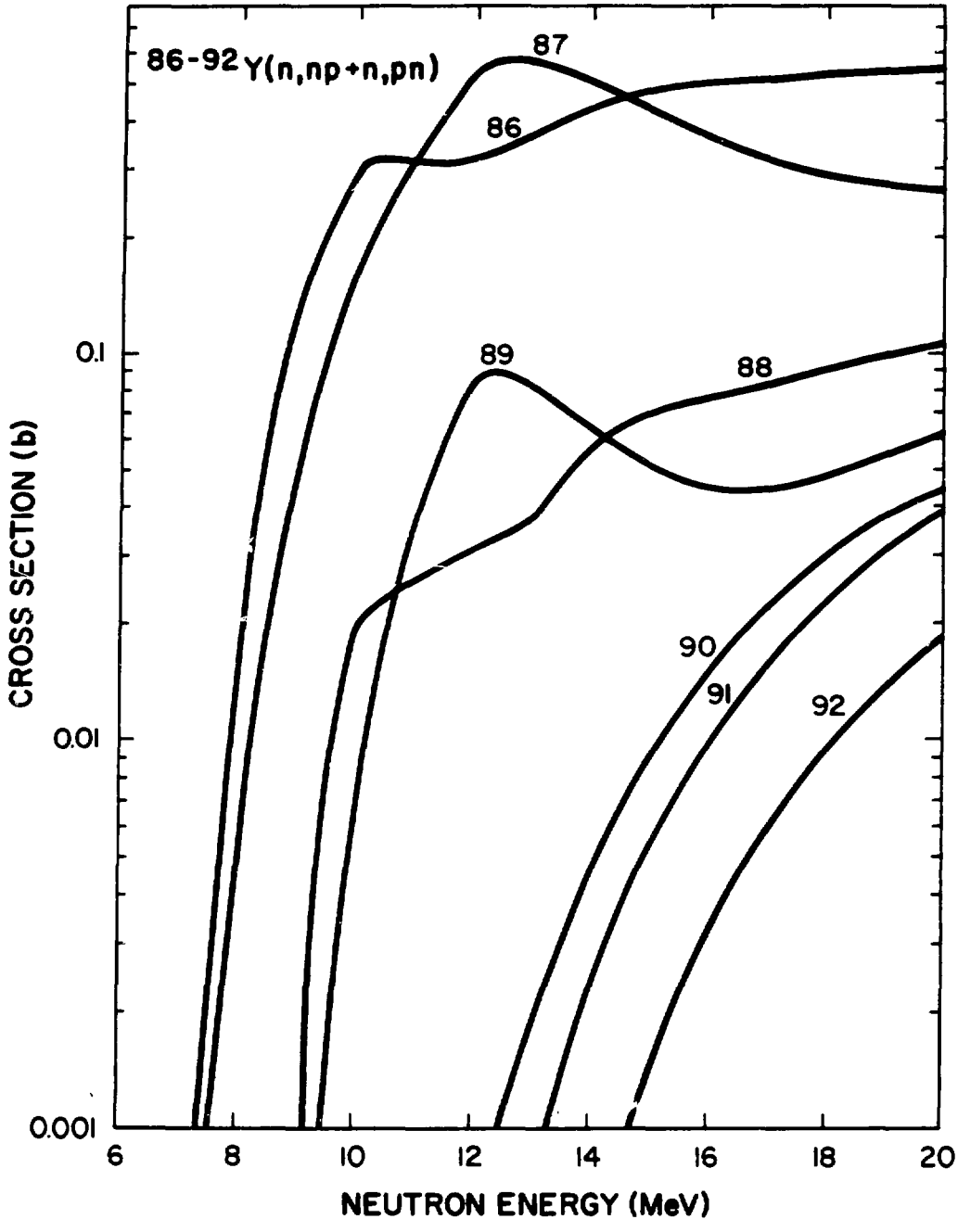

Fig. 4.
Predicted (n,np + n,pn) cross sections for stable and unstable yttrium isotopes.

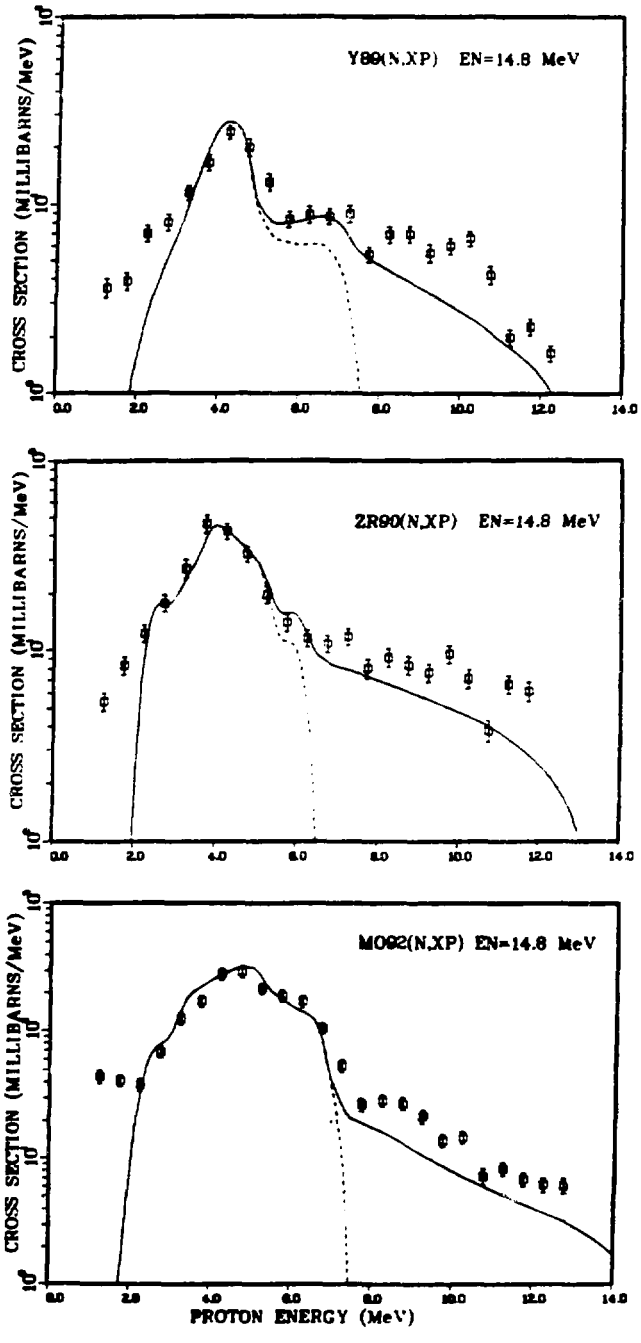

Fig. 5.
A comparison of our calculated proton emission spectra to data measured by Haight et al.[12] The dashed lines represent the sums of contributions from the (n,np) and (n,pn) reactions.

addition, Lagrange's neutron optical parameters[14] applicable to the even-even molybdenum isotopes were used for the ^{92}Mo calculations.

The calculations generally reproduce well the measured data although there are two areas of disagreement occurring at the lower and upper ends of the spectra. To investigate the disagreement occurring for secondary proton energies below 2 MeV, we searched for low-threshold (p,n) experimental data that would be applicable to test the low-energy behavior of our proton optical parameters. The ^{93}Nb(p,n) reaction provides such an opportunity, and Fig. 6 compares our calculation using the proton parameters described above to data[15] measured for this reaction. Two things are noteworthy in this comparison. The first is the extremely small value of the cross section around 2 MeV (1-10 μb) and the other is the ability of the calculation to reproduce the data at these low-incident proton energies. This comparison confirms the sub-Coulomb barrier behavior of our proton optical parameters and makes it difficult to determine a physical explanation for the presence of appreciable amounts of low-energy (<2 MeV) protons in the Haight data, particularly for ^{92}Mo.

To investigate the deviations at higher energies we thought it appropriate to compare the upper portion of the spectra that result primarily from the (n,p) reaction to radiochemical measurements for this cross section. To do so we integrated the upper portion of the spectrum and then subtracted calculated contributions occurring from (n,np + n,pn) reactions given by the dashed lines shown in Fig. 5. The results appear in Table III where radiochemical data are also given. [The total ^{92}Mo (n,p) cross section was estimated using our calculated m/g ratios for ^{92}Nb and the exprimental cross section for ^{92m}Nb production.] The agreement is quite good indicating that there exists a deficiency in our calculations. Such a difference could result from direct-reaction effects that we did not include.

These comparisons have provided an indication of our ability to determine (n,np + n,pn) contributions that constitute the dominant portion of the proton production cross section for neutron energies above 10 MeV. Our agreement with these data provide more confidence in similar cross sections calculated for unstable target nuclei in this mass region.

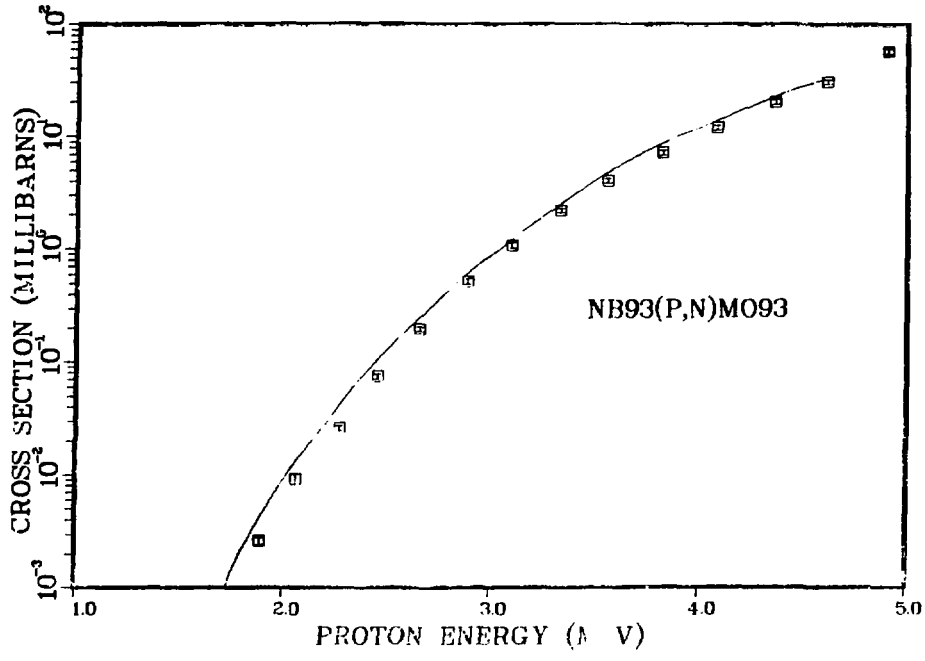

Fig. 6.
Our calculated cross sections are compared to ^{93}Nb(p,n) data in order to test the sub-Coulomb barrier behavior of the proton optical parameters used in the present emission spectra calculation.

TABLE III

(n,p) CROSS SECTIONS DEDUCED FROM MEASURED SPECTRA WITH ALLOWANCE FOR (n,np) AND (n,pn) CONTRIBUTIONS

	Integrated (n,p) (mb)	Radiochemical (n,p) (mb)
^{89}Y	29 ± 3	23 ± 3
^{90}Zr	45 ± 5	45 ± 3
^{92}Mo	98 ± 9	65 ± 6 to ^{92m}Nb (104 estimated total)

F. Determination of Deformed Optical Model Parameters for Neutron Reactions on ^{235}U and ^{239}Pu (E. D. Arthur)

An analysis of several integral assemblies[16] has indicated a possible need to adjust the total inelastic cross section given in the ENDF/B evaluated libraries for ^{235}U and ^{239}Pu, particularly in the incident-neutron energy region around 1 MeV. To see whether an analysis of the available differential data for these nuclei would support possible adjustments, we have begun Hauser-Feshbach statistical model calculations employing neutron transmission coefficients generated from coupled-channel calculations of ^{235}U and ^{239}Pu. Furthermore, we believe a consistent analysis of available experimental data using modern nuclear-model techniques is needed to improve the ENDF data. The most recent analysis incorporating similar methods was that by Prince et al.[17] in 1973 and was only for ^{239}Pu. Since then there have been new high-resolution measurements for elastic and inelastic scattering as well as new total cross-section data.

The first step in this effort has been determination of deformed optical model parameters for use in coupled-channel calculations of direct inelastic scattering as well as to provide coupled-channel transmission coefficients for use in Hauser-Feshbach calculations. To do so we used the ECIS[18] coupled-channel code and coupled together the lower members of the ground-state rotational band for these nuclei (the $\frac{7-}{2}$, $\frac{9-}{2}$, $\frac{11-}{2}$ states for ^{235}U and the $\frac{1+}{2}$, $\frac{3+}{2}$, $\frac{5+}{2}$, $\frac{7+}{2}$, $\frac{9+}{2}$, $\frac{11+}{2}$ levels for ^{239}Pu). For starting values we used the optical parameters determined by Haouat et al.[19] from the analysis of their elastic and inelastic scattering data on ^{232}Th, $^{233\ 235\ 238}U$ and $^{239\ 242}Pu$. We found that for ^{239}Pu in the energy region around 1 MeV the parameters overpredicted somewhat the total cross section. To improve the fit, we adjusted these parameters slightly. The results appear in Table IV. Figure 7 compares the total cross section calculated with these parameters to data available for ^{235}U. In addition, the calculated total cross sections agree well with new measurements by Poenitz.[20]

Transmission coefficients have been generated up to 8 MeV and preliminary Hauser-Feshbach calculations have begun. Efforts are now under way to adjust fission barrier parameters to optimize the fit to the fission cross-section data available for these two nuclei.

TABLE IV

NEUTRON OPTICAL PARAMETERS FOR ^{235}U AND ^{239}Pu
(All depths are in MeV, geometrical parameters in fm)

			r	a
^{235}U	V	= 46.4 - 0.3 E	1.26	0.615
	W_D	= 3.3 + 0.4 E	1.24	0.50
	V_{SO}	= 6.2	1.12	0.47
		β_2 = 0.215 β_4 = 0.075		
^{239}Pu	V	= 46.2 - 0.3 E	1.26	0.615
	W_D	= 3.6 + 0.4 E	1.24	0.50
	V_{SO}	= 6.4	1.12	0.47
		β_2 = 0.21 β_4 = 0.065		

G. Calculation of Excited State Cross Sections for Actinide Nuclei (David G. Madland)

When nuclei in the ground state are placed in a high-temperature environment, such as that occurring in certain astrophysical processes, the number of nuclei existing in excited states may approach a non-negligible equilibrium population relative to the ground-state population. We are attempting to calculate the scattering cross sections for neutron-induced reactions on actinide nuclei existing in low-lying excited states due to such a circumstance.

The first step has been to modify the coupled-channel code JUPITOR[21] to calculate cross sections for members of a rotational band when the target nucleus is in some state other than the band head. This has been accomplished by extensive revision[22] of JUPITOR and has been successfully tested by use of the reciprocity relation. In addition, the code has been modified to calculate the full coupled-channel S matrix, and the symmetry property of the matrix has been explicitly demonstrated in a number of reciprocity test cases. The revised JUPITOR code has been given the local name JUPXST. Further tests and refinements of JUPXST are under way.

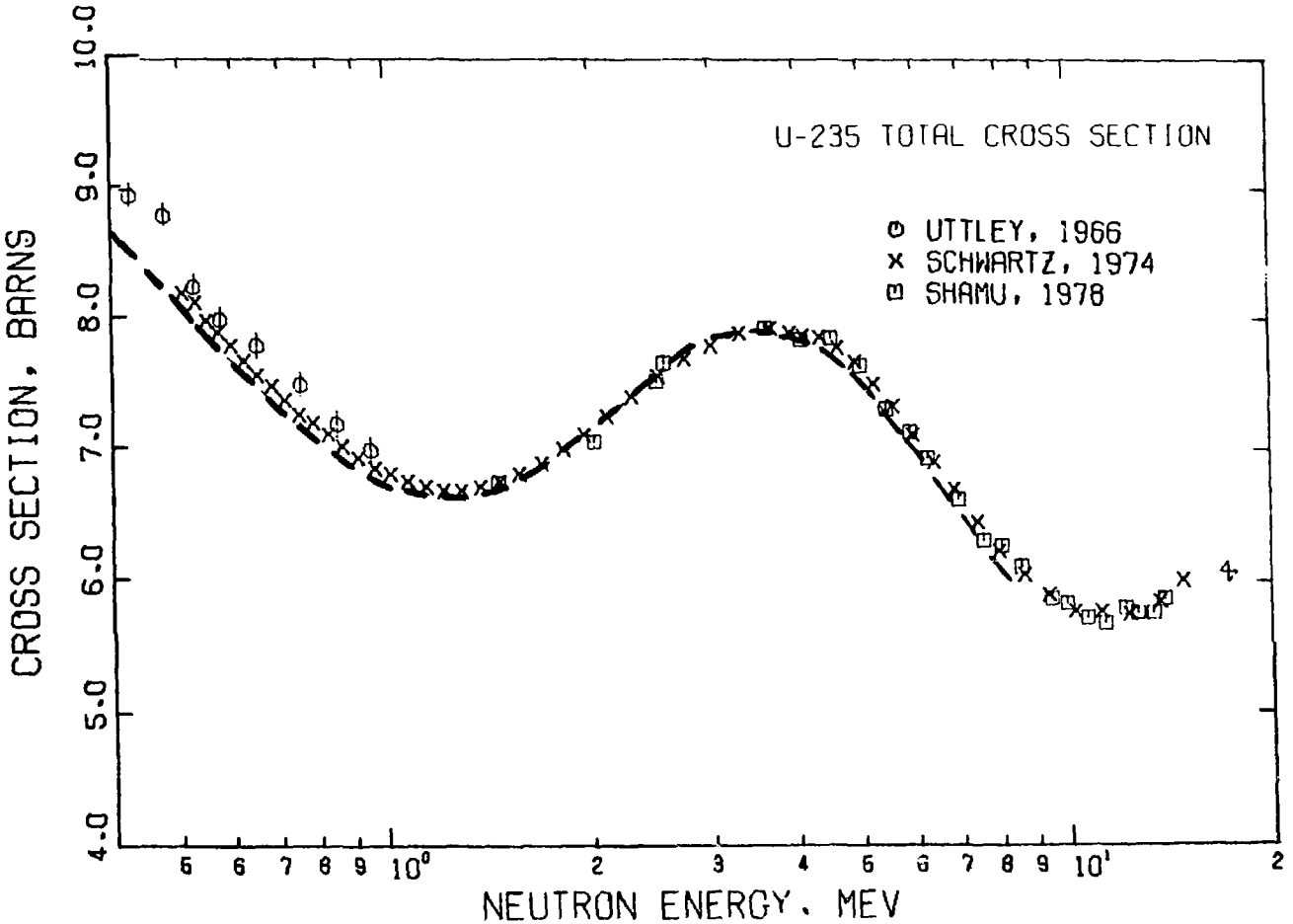

Fig. 7.
Coupled-channel calculations of the ^{235}U total cross section using the optical parameters of Table III are compared to available experimental data.

H. Calculation of the Prompt Neutron Spectrum and $\bar{\nu}_p$ for the Spontaneous Fission of ^{252}Cf (D. G. Madland)

The spontaneously fissioning nucleus ^{252}Cf is used as a standard in several different nuclear measurements. In particular, prompt fission neutron spectra N(E) and average prompt neutron multiplicities $\bar{\nu}_p$ from neutron-induced fission are in many laboratories measured relative to those of the ^{252}Cf(sf) reaction. Results are presented here for the calculation of N(E) and $\bar{\nu}_p$ from ^{252}Cf(sf) using recent developments[23-27] in the theory of prompt fission neutron spectra.

The new calculations account for the effects of (1) the motion of the fission fragments, (2) the distribution of fission-fragment residual nuclear temperature, and (3) the energy dependence of the cross section for the inverse process of compound-nucleus formation. The residual nuclear temperature distribution is based upon the Fermi-gas model and is characterized by a maximum temperature T_m. The compound-nucleus cross section $\sigma_c(\varepsilon)$ is calculated using the optical model. N(E) is given by

$$N(E) = \frac{1}{2}\left[N(E,E_f^L) + N(E,E_f^H)\right] \quad , \tag{1}$$

where

$$N(E,E_f) = \frac{1}{2\sqrt{E_f}T_m^2} \int_{u_1 T_m}^{u_2 T_m} \sigma_c(\varepsilon)\sqrt{\varepsilon}\, d\varepsilon \times \int_0^{T_m} c(T)\, T \exp(-\varepsilon/T) dT \quad , \tag{2}$$

with E and ε the laboratory and center-of-mass energies, respectively, of the emitted neutron; T the residual nuclear temperature; c(T) the normalization integral; E_f the kinetic energy per nucleon in either the light (L) or heavy (H) fragment; $u_1 = (\sqrt{E} - \sqrt{E_f})^2/T_m$, and $u_2 = (\sqrt{E} + \sqrt{E_f})^2/T_m$.

The expression for $\bar{\nu}_p$ is given by

$$\bar{\nu}_p = \frac{\langle E^* \rangle - \langle E_\gamma^{tot} \rangle}{\langle S_n \rangle + \langle \varepsilon \rangle} \quad , \tag{3}$$

where $\langle E^* \rangle = aT_m^2$ is the initial total average fission-fragment excitation energy, $\langle E_\gamma^{tot} \rangle$ is the total average prompt gamma-ray energy, $\langle S_n \rangle$ is the average fission-fragment neutron separation energy, and $\langle \varepsilon \rangle$ is the average energy of the center-of-mass neutron spectrum. The level-density parameter is given by a = A/(11 MeV), where A = 252.

It is clear from Eqs. (2) and (3) that N(E) and $\bar{\nu}_p$ should be calculated and compared to experiment simultaneously because they both depend strongly upon T_m.

Gaussian quadrature is used to evaluate the three numerical integrals of Eq. (2). A more simple, but also less exact, spectrum is obtained by assuming $\sigma_c(\varepsilon)$ constant and simulating its energy dependence by adjusting the level-density parameter to some new value a_{eff}. In this case N(E) is a closed expression given by Eq. (1) with

$$N(E,E_f) = \frac{1}{3\sqrt{E_f T_m}} \left[u_2^{3/2} E_1(u_2) - u_1^{3/2} E_1(u_1) + \gamma(3/2,u_2) - \gamma(3/2,u_1)\right], \quad (4)$$

where $E_1(x)$ is the exponential integral,[28] $\gamma(a,x)$ is the incomplete gamma function,[28] and T_m is calculated using a_{eff}. The average center-of-mass energy corresponding to Eqs. (1) and (4) is $\langle \varepsilon \rangle = (4/3)T_m$.

Thus, N(E) can be obtained exactly by using Eqs. (1) and (2) or approximately by using Eqs. (1) and (4). In either case, three input parameters--E_f^L, E_f^H, and T_m--are required.

The results using both formalisms are summarized in Fig. 8 and Table V. In Table V, the input parameters E_f^L and E_f^H are obtained from Unik et al.,[29] and T_m is determined from the difference between the average fission Q value[30,31] and the total average fission-fragment kinetic energy.[29] The mean energy and mean-square energy of the center-of-mass and laboratory prompt neutron spectrum are tabulated together with $\bar{\nu}_p$ calculated using $\langle S_n \rangle = 5.473$ MeV from Refs. 30, 31, and $\langle E_\gamma^{tot} \rangle = 6.95$ MeV from Ref. 32. Also given are the parameters A_{Watt} and B_{Watt} of the Watt spectrum[33] as derived from the appoximate formalism assuming equal mean laboratory energies. The calculated spectra are compared to the experimental measurement of Boldeman et al.[34] in Fig. 8. It is clear from Fig. 1 that good agreement exists between the calculated and measured spectra. A close examination of the peak region on a linear scale, however,

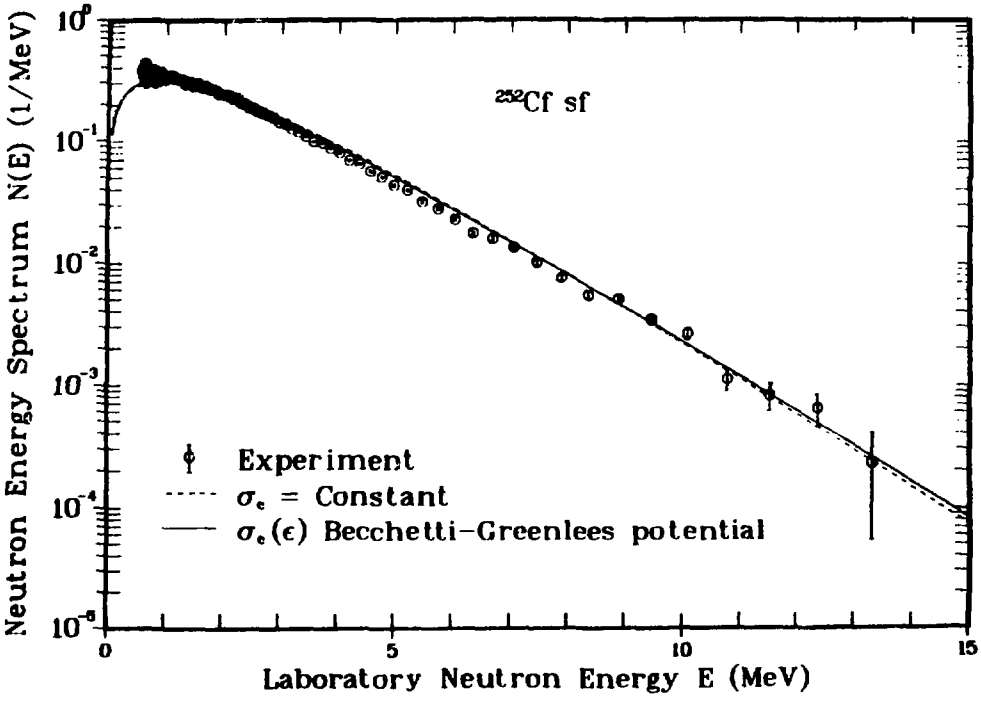

Fig. 8.
Prompt fission neutron spectrum for the spontaneous fission of ^{252}Cf. The dashed curve gives the simulated energy dependence of $\sigma_c(\epsilon)$ result using Eqs. (1) and (4) with a_{eff} = A/(10 MeV), whereas the solid curve gives the exact energy-dependent σ_c calculations using Eqs. (1) and (2) with the optical-model parameters of Becchetti and Greenlees.[35] The experimental data are those of Boldeman et al.[34]

shows a clear preference for the exact energy-dependent calculation using the optical-model potential of Becchetti and Greenlees.[35] The current[36] average measured value of ν_t is 3.766, corresponding to ν_p = 3.757, which is in excellent agreement with the calculated values.

I. International Nuclear Model Codes Comparison Study (D. G. Madland)

The coupled-channel exercise distributed by Enrico Sartori of the OECD/NEA Nuclear Data Bank has been calculated using the code JUPITOR.[21] The version of the code used is one in which no modifications exist other than correction of known errors. The results obtained together with compiled and execution times have been sent to Sartori for the code comparison study.

TABLE V

SUMMARY OF CALCULATIONS[a]

Present Calculation

Quantity	Energy-Dependent Calculation	Simulated Energy Dependence
E_f^L	0.984	0.984
E_f^H	0.553	0.553
T_m	1.209	1.153
$\langle \varepsilon^2 \rangle$	3.956	3.989
$\langle E \rangle$	2.279	2.306
$\langle E^2 \rangle$	8.455	8.564
$\overline{\nu}_p$	3.803	3.788

Watt Distribution

Quantity	Value
A_{Watt}	1.025
B_{Watt}	2.926
$\langle E \rangle$	2.306
$\langle E^2 \rangle$	8.469

[a]Energies and temperatures are expressed in MeV.

II. NUCLEAR CROSS-SECTION PROCESSING

A. An Improved Calculation of Heating and Radiation Damage from Neutron Capture (R. E. MacFarlane).

The current version of the NJOY code computes the recoil distribution of the residual nucleus of the radiative capture cross section by energy balance; that is,

$$E_R = E + Q - E_\gamma(E) \quad , \tag{5}$$

where E_R is the recoil energy, E is the incident neutron energy, Q is the reaction Q value (positive), and E_γ is the total energy of the capture photon spectrum. This formula has two main problems. First, it breaks down for elements where the effective Q is an energy-dependent weighted average of the Q values of the various isotopes. Second, E_R is small at low energies, so Eq. (1) represents a difference between large numbers that requires extraordinary precision in giving the photon spectrum. As a result, it is not unusual to find absurdly large or small (even negative) values of E_R for the ENDF files.

This is not always a problem when the heating KERMA factors are being computed for isotopes because Eq. (5) explicitly conserves energy. Moderate errors in E_R will be compensated for by the corresponding error in E_γ. The total heating will always be correct, but the spatial distribution of heat can be distorted. For radiation damage, however, the entire effect comes from E_R and significant errors can result from using Eq. (5).

For these reasons, the HEATR module of NJOY is being modified to use momentum conservation to compute the recoil. By kinematics, the recoil energy is

$$E_R = \frac{E}{A+1} - 2\sqrt{\frac{E}{A+1}}\sqrt{\frac{E_\gamma^2}{2(A+1)mc^2}}\cos\phi + \frac{E_\gamma^2}{2(A+1)mc^2} \quad , \tag{6}$$

where E is the incident neutron energy, E_γ is the energy of the photon emitted at angle ϕ, A is the target mass ratio to the neutron, and mc^2 is the neutron mass-energy. The average over all angles assuming isotropy is

$$E_R = \frac{E}{A+1} + \frac{E_\gamma^2}{2(A+1)mc^2} \quad . \tag{7}$$

The second term begins to be important below 25-100 keV. If subsequent photons are emitted (cascade), each one will add additional terms in E_γ^2, and the last term can be written using $\overline{E_\gamma^2}$. Therefore, Eq. (7) gives a result for E_R that works for both elements and isotopes and has no precision problems. However, it no longer conserves energy, and materials with bad photon data can still cause problems.

The atomic displacements produced by the recoil nucleus depend on a nonlinear function of E_R, and averaging Eq. (7) becomes a complex calculation. However, damage calculations are still fairly crude, and the upper esitmate for the damage obtained by treating the neutron "kick" and the photon kick independently should be accurate for all practical calculations because

$$\int_{-1}^{1} D(E_R)\, d\cos\theta \leq D\left(\frac{E}{A+1}\right) + D\left(\frac{\overline{E_\gamma^2}}{2(A+1)mc^2}\right) . \qquad (8)$$

HEATR still computes the KERMA factor and damage energy cross section for other reactions by energy balance, and kinematic checks can still be used to find evaluations with severe energy-balance problems.[37] It was recently discovered that photon kick damage was also considered by Gabriel, Amburgey, and Greene,[38] but they used a Monte Carlo calculation based on data from the Nuclear Data Sheets rather than the approximate integration of the ENDF/B photon distribution functions indicated here.

B. LMFBR Cross-Section Production with MAX (R. E. MacFarlane)

For the past several years, the Office of Reactor Research and Technology of the U. S. Department of Energy has sponsored the Large-Core Code Evaluation Working Group (LCCEWG), which has been making inter-laboratory comparisons of the multi-dimensional diffusion, transport, and burnup codes that are currently used for fast-reactor analysis and design. In order to focus the checks onto these codes, a single set of cross sections was used. They were prepared by the General Electric Company's (GE) Advanced Reactor Systems Development group using the TDOWN-IV code.[39]

During this quarter, the MAX macroscopic cross-section system was used to prepare a similar set of cross sections and to extend the set by including P_1 anisotropy. The purposes of this exercise were to provide P_1 cross sections for the Transport Theory Group (T-1) at Los Alamos by calculation of the benchmark,

to check the usefulness of MAX for realistic problems, and to provide an estimate of the sensitivity of the benchmark to different processing methods.

LCCEWG Benchmark 3 is a 1000-MWe heterogeneous LMFBR with mixed-oxide driver fuel and uranium-oxide blankets. The goal of the calculation is to provide 4-group cross sections for each material with self-shielding and flux collapse appropriate to each region of the reactor. The first step was to prepare 70-group self-shielded cross sections for the driver, blanket, control, and structure regions using TRANSX.

The driver element consists of a hexagonal duct of stainless steel containing 271 stainless-clad fuel pins. For consistency with GE, the flux was taken to be flat throughout the assembly (that is, advantage and disadvantage effects were neglected). The escape cross section from the fuel pins was calculated for an infinite hexagonal lattice using the Sauer approximation to the Dancoff correction. The interstitial sodium was shielded using a mean-chord equal to the fuel mean-chord transformed by the moderator-to-fuel volume ratio and no Dancoff correction. The clad, duct wall, and sodium inside and outside of the duct were treated as slabs of various thicknessess. Both macroscopic and microscopic cross sections were generated.

A similar calculation was made for the blanket element. The control region with the rods out and the structure were treated as simple homogeneous regions. The preceding steps required a total of four TRANSX runs.

The next step was to use a new utility code called XSX to extract the macroscopic cross section for each of the four regions from the corresponding TRANSX output file and merge them into a single group-ordered library for the ONEDA module of MAX. This code is a modified and extended version of the T-1 diffusion-accelerated one-dimensional transport code ONEDA (since superseded by ONEDANT).[40] It was used to perform a diffusion flux solution for a simplified one-dimensional model of the benchmark.

Finally, the 70-group diffusion flux by regions was used in XSX together with the output of the four TRANSX runs to collapse the microscopic cross sections into separate 4-group sets for each region. The results were produced directly in ISOTXS format.

A total of three cross-section sets were produced in this way: (1) P_0 cross sections collapsed with the diffusion flux, (2) P_0 cross sections collapsed with the P_0S_8 flux, and (3) P_1 cross sections collapsed with the P_1S_8 flux. The 70-group ONEDA eigenvalue for each of these calculations is given in Table VI.

The 4-g.oup libraries were then used in ONEDANT to make the same calculation with the results quoted in the last column. The difference between the columns may be partly an effect of group size and partly due to somewhat different buckling corrections. The differences between the rows are more interesting. The ONEDANT P_0S_8 runs show that it is not necessary to collapse with a transport flux to get good coarse-group cross sections for transport. The ONEDA and ONEDANT runs both show that the difference between transport and diffusion is important and that the difference between P_0 and P_1 is not. The Δk seen here is about twice as large as the difference betwen diffusion and transport seen in the 2-d code comparisons, so the one-dimensional model may exaggerate the transport effects. However, the qualitative conclusions stated above should still hold.

The comparisons with the GE results are still in progress. The high energy results are in good agreement (the same basic library was used). The fuel shielding factors show a small bias, possibly due to the use of infinite lattice Dancoff corrections t' t neglect the effect of the extra sodium and steel in the duct. The structure shielding factors cannot be compared directly because of the different accounting used. The most noticeable difference in the cross sections was in ^{238}U resonance capture. It was traced to a problem in the TDOWN methd for interpolating in the shielding factor tables, which has since been fixed.

TABLE VI

COMPARISON OF VARIOUS ONE-DIMENSIONAL TRANSPORT MULTIPLICATION CALCULATIONS FOR LCCEWG BENCHMARK 3

Set	ONEDA[a]		ONEDANT[b]	
1	Diffusion	1.0086	P_0S_8	1.0213
2	P_0S_8	1.0151	P_0S_8	1.0212
3	P_1S_8	1.0145	P_1S_8	1.0198

[a] 70-group Los Alamos T-2 calculations.

[b] 4-group Los Alamos T-1 calculations made by D. Marr.

C. TRANSX Development (R. E. MacFarlane)

The realistic LMFBR cross-section calcuation described in Sec.II-B revealed several inefficiencies and inconveniences in the current version of TRANSX (version 2). This has led to some important changes in the developmental version 3 described in the previous report of this series, and the result has been renumbered as version 4.

The following changes were made. The input format was modifed to make the specification of regions for self-shielding and the identification of constituent cross sections easier. The calculation of shielding interpolation factors was consolidated so the factors computed while processing the vector cross sections can also be used for the matrix cross sections. An error in the self-shielding of photon production for coupled sets was repaired. The slab cell heterogeneity option was extended to allow both reflective and periodic cell definitions. The flux printout was improved. And, finally, some cleanup of coding and statement number sequencing was carried out.

This experimental version is available to Los Alamos users on the Common File System as /TRANSX/NEW/X4. The source file is S4 on the same root. Version 4 should be used with the new format libraries such as /TRANSX/NEW/MATXS6.

D. THOR Calculations (R. B. Kidman)

It has previously been noted that the calculated eigenvalues for the Los Alamos reflected assemblies are relatively high. Because the THOR benchmark exhibits one of the highest computed eigenvalues (K = 1.0152), it was selected for further study in an effort to reduce the discrepancy.

It has also been reported that utilizing P_5 instead of just P_3 cross sections increased the eigenvalue by 0.0026 to 1.0178.

This past quarter we were able to test the effect of utilizing region-dependent chi matrices instead of a single vector chi. Even though there were substantial differences between these chi representations, the region-dependent fission-source matrices lowered the THOR eigenvalues by only 0.0017 to 1.0161.

Several other options (such as varying the group structure, varying the angular quadrature, using self-shielded cross sections) were judged to have negligible effect on the THOR eigenvalue since they had negligible effect on the JEZEBEL and GODIVA eigenvalues.

Finally, the process of reducing the actual experimental THOR assembly to clean benchmark specifications was reviewed. Our somewhat independent attempt

at this process gave new specifications that lowered the THOR eigenvalue by only 0.0055 to 1.0106.

Thus the high eigenvalue discrepancy has not yielded to any general calculational improvement, nor is it likely that improved benchmark specifications will solve the problem. The eigenvalue remains about 1% high. Unfortunately, even though cross sections have gone through years of adjustment, it appears that a resolution of Los Alamos reflected assembly eigenvalues will require yet another round of delicate, interdependent changes of the involved isotope cross sections.

E. Covariance Processing (D. W. Muir)

ERRORR, the NJOY covariance processing module, has been extended to treat ENDF/B File 31, which contains uncertainties and correlations in energy-dependent fission $\bar{\nu}$ values. Multigroup covariances were calculated for all $\bar{\nu}$ data included in the ENDF/B-V evaluation for ^{238}U (MAT 1398). This calculation included the cross-material covariances of ^{238}U $\bar{\nu}$ values (prompt, delayed, and total) with total $\bar{\nu}$ values of five other materials, namely ^{232}Th (MAT 1390), ^{235}U (MAT 1395), ^{239}Pu (MAT 1399), ^{240}Pu (MAT 1380), and ^{241}Pu (MAT 1381). The processing of these latter covariances required the addition of general cross-material logic to ERRORR. This will be a useful feature when cross-material covariances appear in other ENDF/B evaluations, as planned for example in future versions of the ENDF/B dosimetry library.

Minor changes were also made in the NJOY covariance plotting program CPL in order to accomodate $\bar{\nu}$ uncertainties. Figures 9, 10, and 11 show CPL-generated plots of the multigroup covariances of ^{238}U (prompt ν) with ^{238}U (prompt ν), those of ^{238}U (delayed ν) with ^{238}U (delayed ν), and those of ^{238}U (total ν) with ^{240}Pu (total ν).

F. Analysis of Charges for Use of Central Computing Facility (D. G. Foster, Jr.)

For the past 7 yr, the Nuclear Data Group has found it desirable to examine the details of its charges for the use of the Los Alamos Central Computing Facility (CCF), primarily in order to monitor the costs of specific projects within each program code. This has been accomplished using a simple computer code ACCT, which we have been forced to modify almost every year as the CCF accounting system has changed and grown in complexity. At the beginning of

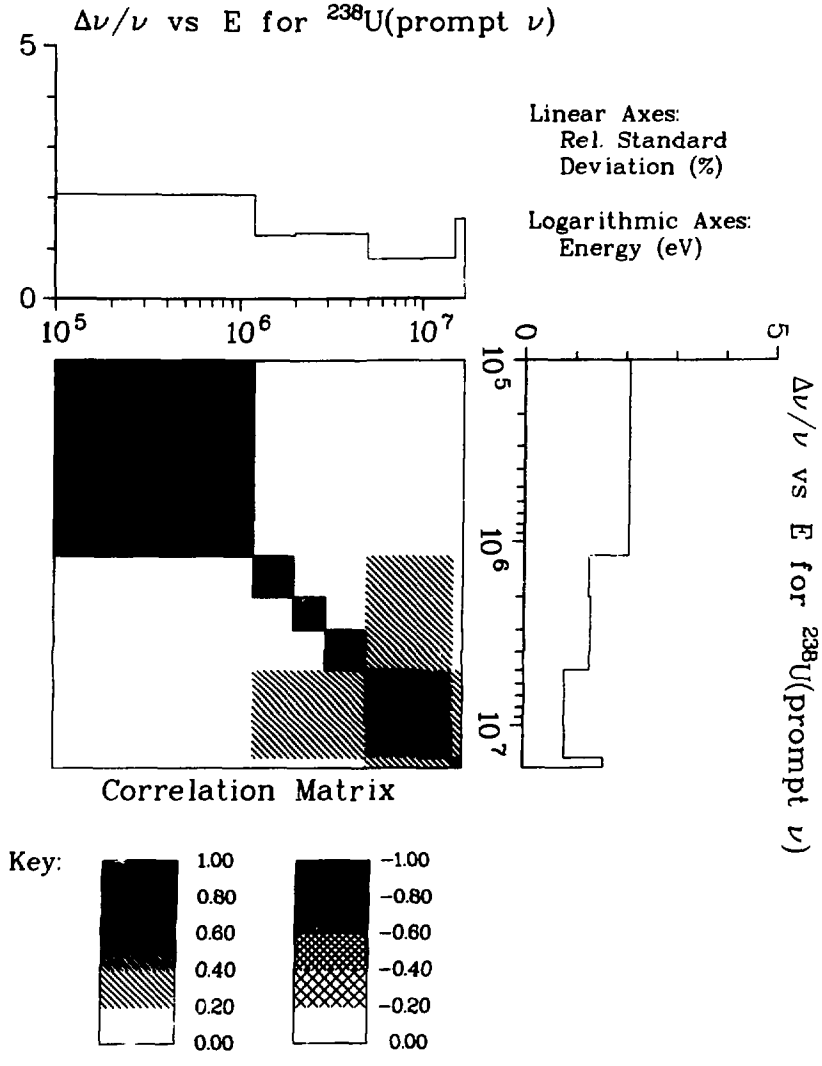

Fig. 9.
Covariance data for ^{238}U (prompt ν) with ^{238}U (prompt ν).

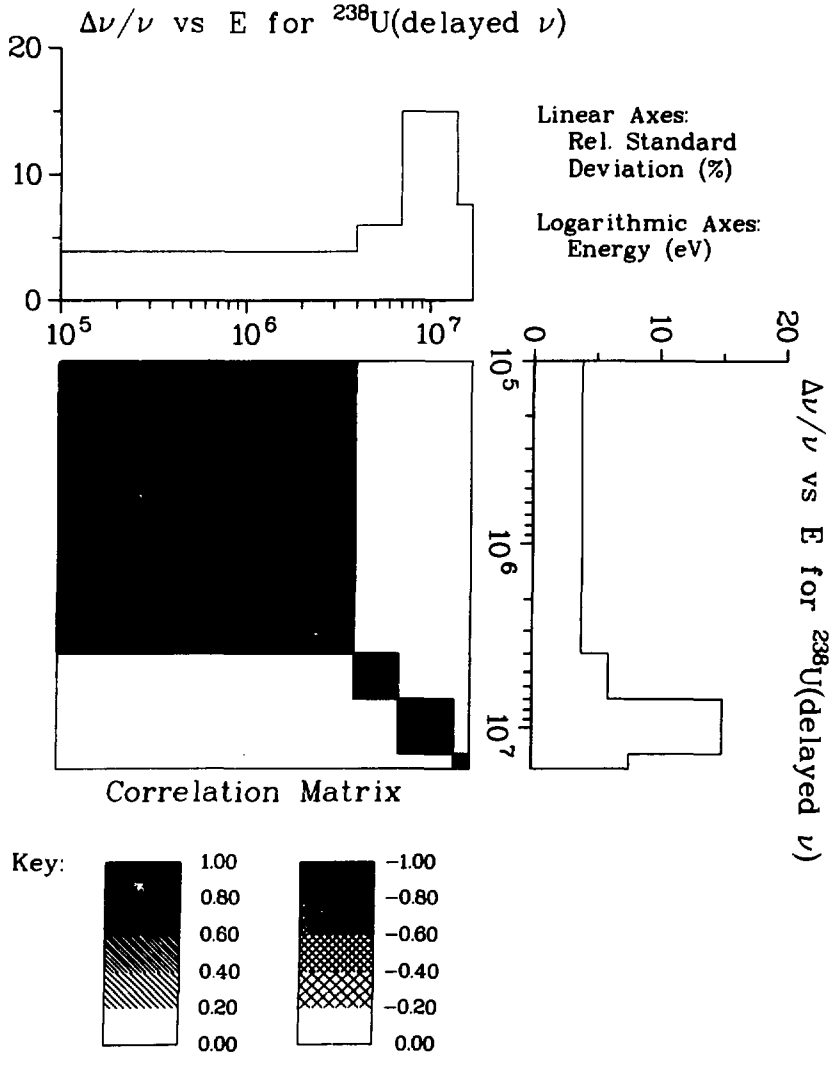

Fig. 10.
Covariance data for ^{238}U (delayed ν) with ^{238}U (delayed ν).

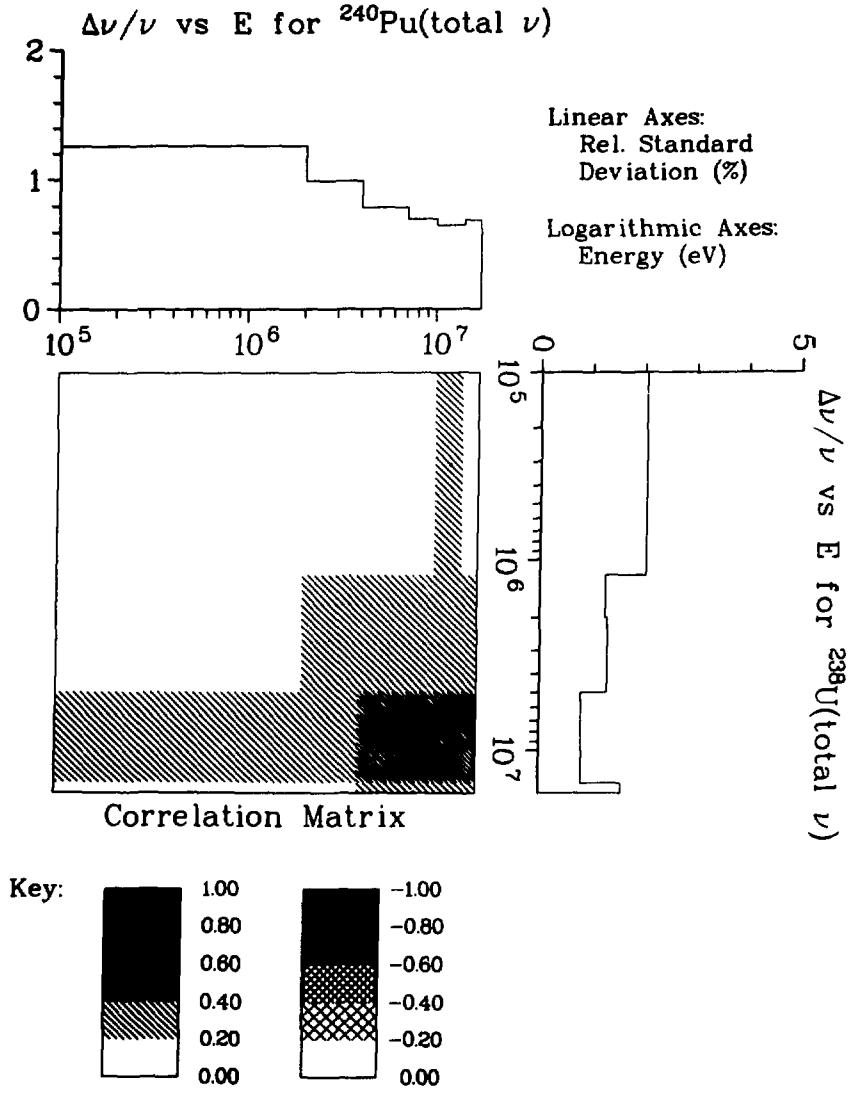

Fig. 11.
Covariance data for ^{238}U (total ν) with ^{240}Pu (total ν).

fiscal year 1981, the system was expanded drastically and data on explicit charges for devices other than the CCF-worker computers became available to the users through the Common File System. Accordingly, we have rewritten ACCT . . . almost completely, and simultaneously made it available to other groups in the Laboratory.

The addition of new groups, each with its own pattern of CCF use, has allowed us to debug ACCT much more thoroughly than in the past and has called attention to errors in the accounting system itself. It has also spotlighted opportunities to reduce future charges to T Division by several thousand dollars per month.

G. S_n Calculations for D_2O Sphere (R. J. LaBauve, D. C. George, and D. G. Madland)

In response to a request from C. Eisenhauer of the National Bureau of Standards (NBS), a series of discrete ordinate calculations was run for a 15-cm radius D_2O ("heavy water") sphere. The Los Alamos National Laboratory discrete ordinates code ONEDANT[40] and cross sections for ^2H and ^{16}O from ENDF/B-V[41] as processed by the NJOY[42] code were used in these calculations. The multigroup data from NJOY were in 150 energy groups with a Legendre expansion = P_3. Additional input specifications to the ONEDANT code were as follows.

Quadrature - S_{32}

Mesh - 10 points from 0 to 0.1 cm, 100 points from 0.1 to 15 cm, and 1 point at 15.01 cm. The point outside the D_2O sphere was used for observing the "leakage spectrum."

Atom densities - a density of 1.10534 was used for D_2O at 20° C.[43]

Fission source - central volume ^{252}Cf source. Two representations of the ^{252}Cf spontanteous fission spectrum were used. One was an evaluation by NBS.[44] The other was derived from a theoretical model[25] developed at Los Alamos.

Results are shown in Figs. 12-25. Figures 12 and 13 show the ^{252}Cf spontaneous fission spectrum as evaluated at NBS. Note that the 150 neutron energy groups were truncated at about 10 eV. This was done for comparison purposes as the Los Alamos representation does not extend below 10 eV. Also, for purposes of comparison, a zero value for group 1 of the NBS spectrum was replaced with 1.1×10^{-5}, approximately the value in group 1 of the Los Alamos spectrum.

The Los Alamos calculation of the ^{252}Cf spontaneous-fission spectrum requires a calculation of the average prompt-fission Q value. Originally, this calculation was done using the measured nuclear masses as compiled by Wapstra and Bos [30] where available, and otherwise the mass formula of Myers.[31] More recently we have calculated the prompt-fission Q value, again using the Wapstra and Bos measured values where available, but otherwise the Moller-Nix formula.[45] Figure 14 shows a comparison of the original Los Alamos spectrum with the NBS spectrum, that is, (NBS value - Los Alamos value)/(NBS value) x 100. Note that except for the value at 10 eV, which generally should be discounted, the two spectra are in very good agreement up to about 10 keV. The per cent difference then increases to a maximum, that is, the NBS spectrum is greater than that of Los Alamos at 0.25 MeV and then the difference falls to zero at about 1.7 MeV. At greater energies (where the Los Alamos spectrum is greater than the NBS spectrum), the absolute difference increases rapidly. The difference at 20 MeV should, of course, be ignored.

Figure 15 shows a comparison of the two Los Alamos representations of the ^{252}Cf spontaneous-fission spectrum, and Fig. 16 shows a comparison of the second Los Alamos representation with the NBS evaluation. Note, however, that only the first of the two Los Alamos representations was used in the D_2O sphere calculation.

Figures 17 and 18 show the isotropic flux "leakage spectrum" resulting from the ONEDANT calculations. Figure 19 is a comparison of leakage spectra using the original Los Alamos and NBS representations of the ^{252}Cf source. Note that the 20% difference observed in Fig. 14 at 0.25 MeV is no longer evident and, instead, there is a constant 3% difference to about 0.25 MeV. This 3% difference is due to downscatter from higher energies. The NBS spectrum contributes more neutrons from energies in the interval 10 keV to 1.7 MeV, and it is interesting to observe how this effect develops as a function of sphere radius.

Figure 20 shows the flux comparison for the first space interval from 0.0 to 0.01 cm. In this interval, the flux is essentially "uncollided," and the comparison is practically identical to that for the two spectra shown in Fig. 14. Figure 21 shows the flux comparison for the eighth interval (0.07 to 0.08 cm) in which the 3% difference caused by downscatter is evident. Finally, Fig. 22 in this series shows how the 3% difference develops as a function of radius for a particular group (group 142 from 101.3 to 167 eV).

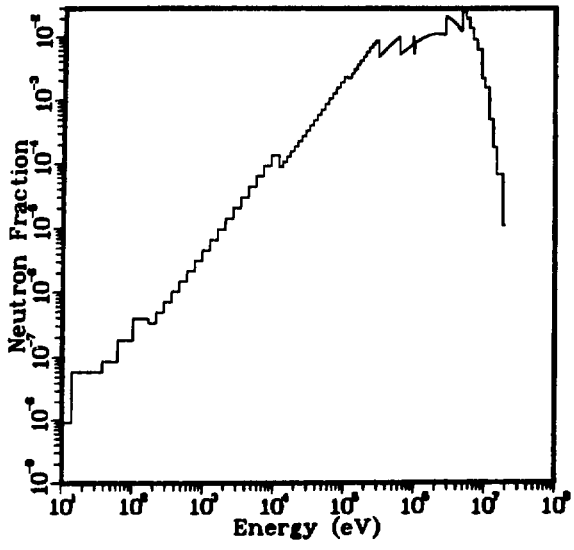

Fig. 12.
^{252}Cf spontaneous fission spectrum, NBS evaluation.

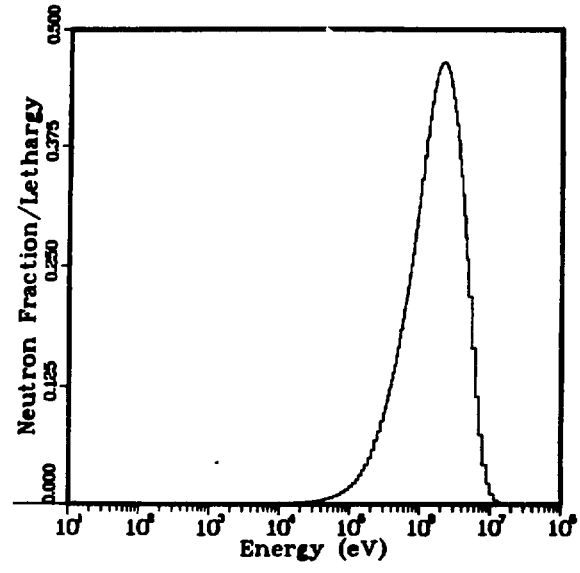

Fig. 13.
^{252}Cf spontaneous fission spectrum in units of neutron fraction/lethargy, NBS evaluation.

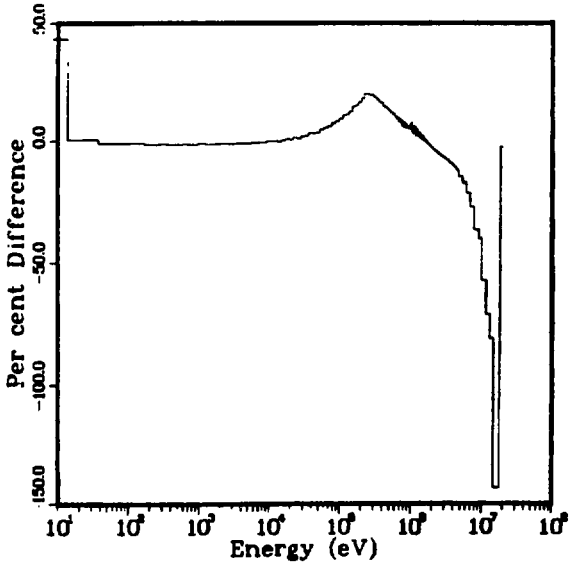

Fig. 14.
Comparison of first Los Alamos $^{252}Cf(sf)$ spectrum with the NBS ^{252}Cf fission spectrum.

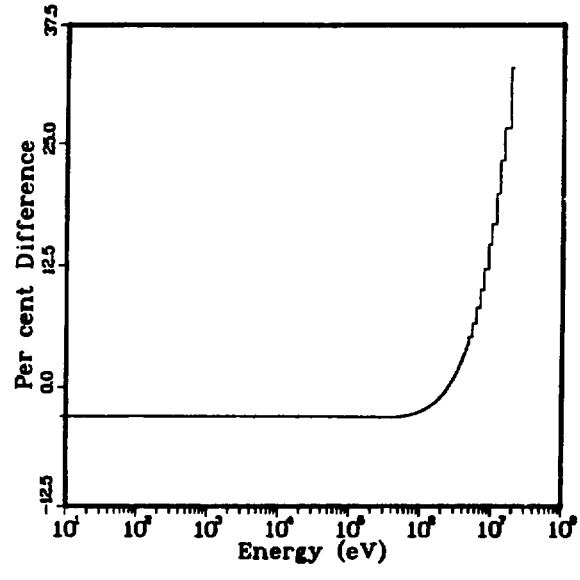

Fig. 15.
Comparison of two Los Alamos calculations of the $^{252}Cf(sf)$ spontaneous fission.

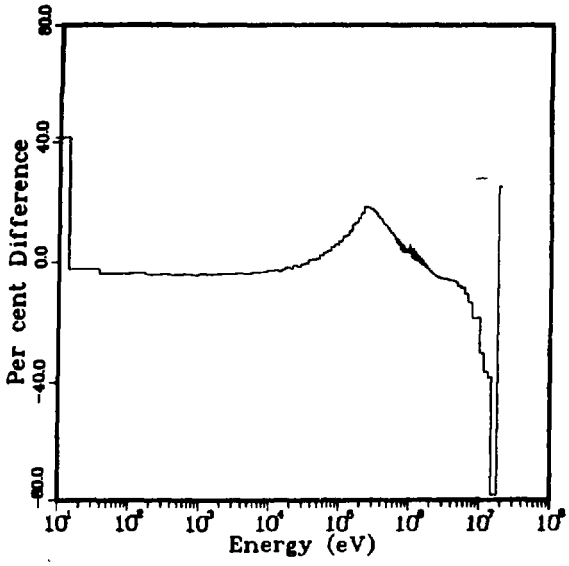

Fig. 16.
Comparison of the NBS evaluation of the ^{252}Cf spontaneous fission spectrum with the second Los Alamos ^{252}Cf spectrum calculated.

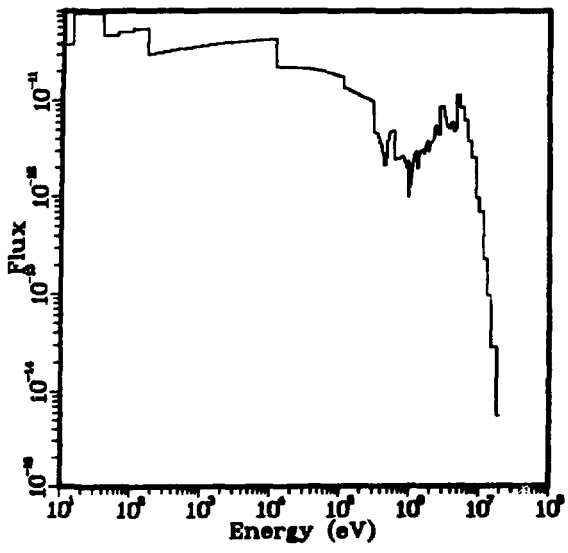

Fig. 17.
Leakage spectrum from 15 cm D_2O sphere with ^{252}Cf spontaneous fission source at center.

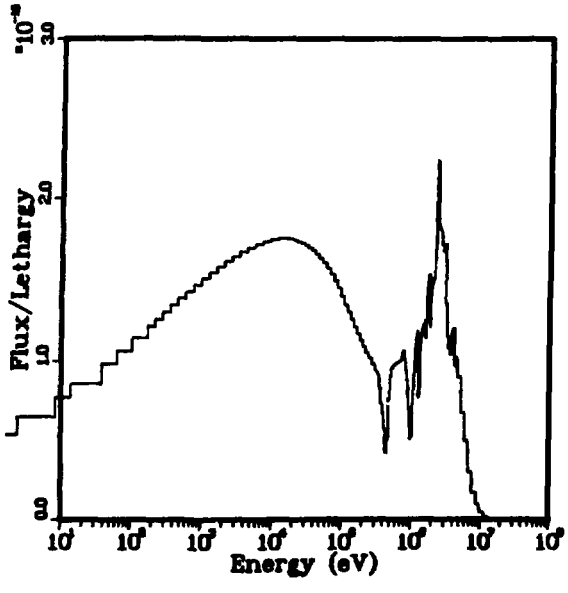

Fig. 18.
Leakage spectrum from D_2O sphere in units of flux/lethargy.

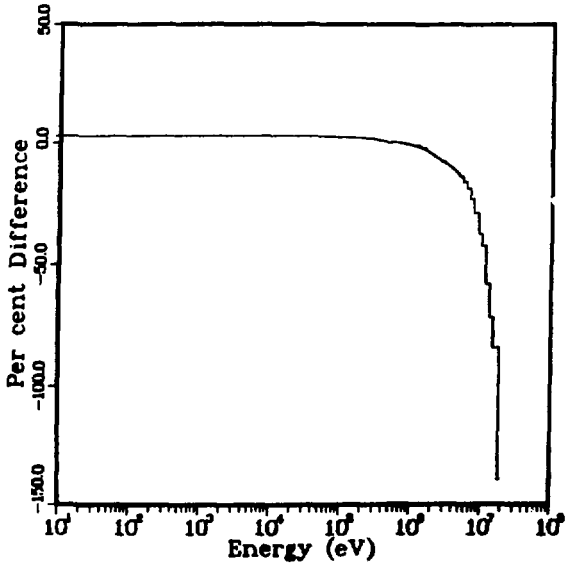

Fig. 19.
Comparison of leakage spectra resulting from using Los Alamos and NBS representations of ^{252}Cf source.

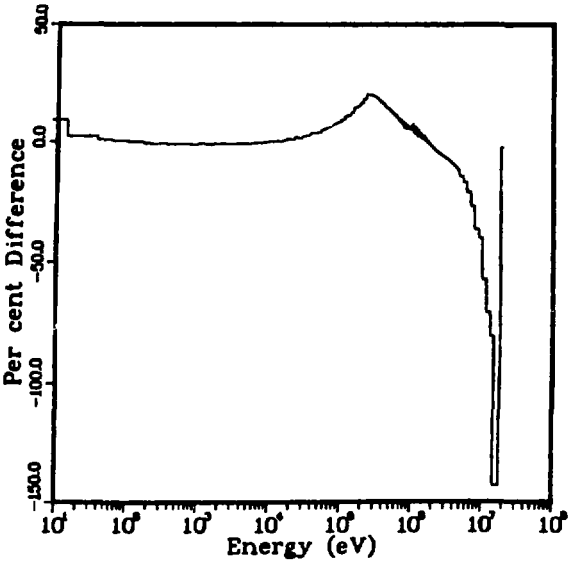

Fig. 20.
Flux comparison for first space interval, 0.0-0.01 cm.

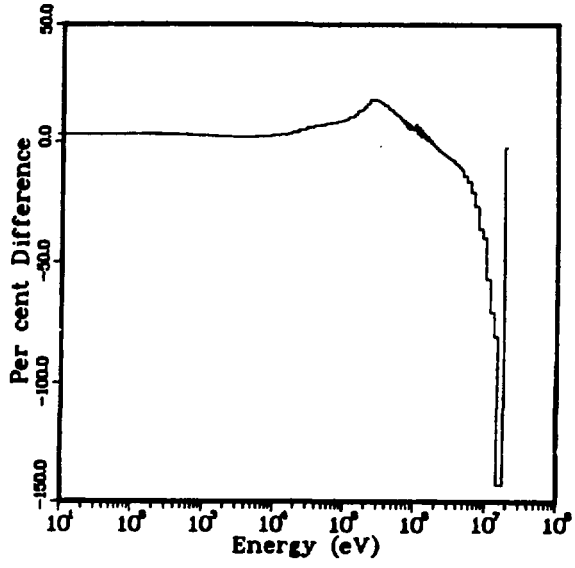

Fig. 21.
Flux comparison for the eighth space interval, 0.07-0.08 cm.

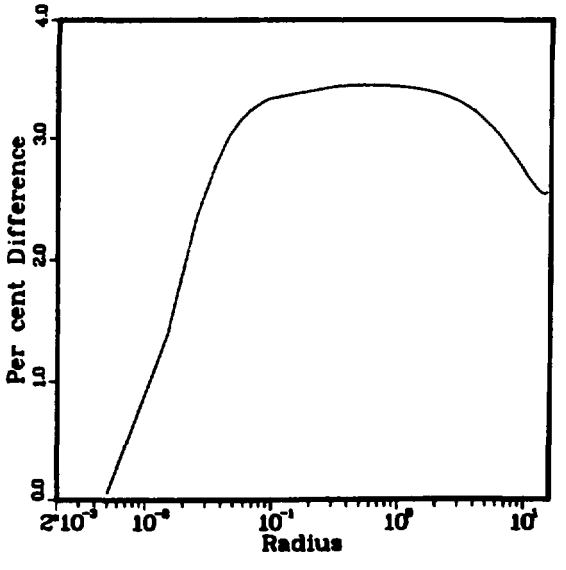

Fig. 22.
Flux comparison in group 142 (101.3 to 167 eV) as a function of radius.

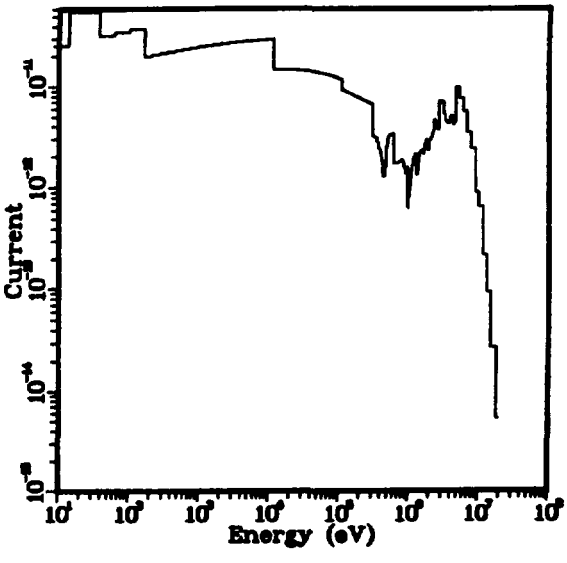

Fig. 23.
Spectrum of leakage current (P_1 moment of flux) from 15 cm D_2O sphere with ^{252}Cf spontaneous source at center.

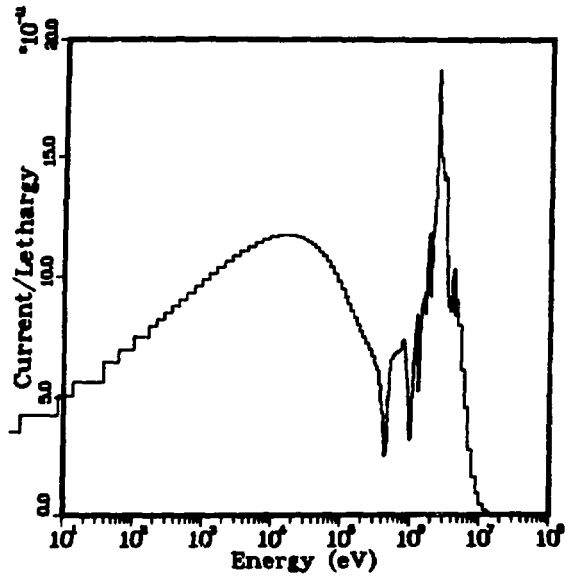

Fig. 24.
Leakage current spectrum from D_2O sphere in units of current/ lethargy.

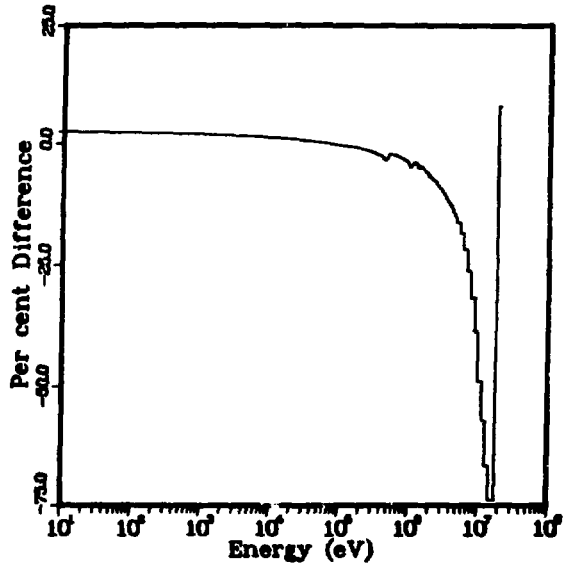

Fig. 25.
Comparison of leakage current spectra resulting from using Los Alamos and NBS representations of ^{252}Cf source.

Figures 23 and 24, in units of current and current/lethargy, respectively, show the spectrum of the leakage "current" or P_1 moment of the flux, from the calculations using the NBS representation of the ^{252}Cf spontaneous fission spectrum. Figure 25 is a comparison of leakage current spectra resulting from using Los Alamos and NBS ^{252}Cf sf representations. Results are similar to those comparisons of the isotropic flux seen in Fig. 19.

III. FISSION PRODUCTS AND ACTINIDES: YIELDS, DECAY DATA, DEPLETION, AND BUILDUP

A. Integral Data Testing of ENDF/B Fission-Product Data (R. J. LaBauve, D. C. George, and T. R. England)

Four experiments, three from Oak Ridge[46] in which ^{235}U samples were irradiated with thermal neutrons for 1, 10, and 100 s, respectively, and one from Los Alamos[47] in which the irradiation time was 5.56 h (20 000 s) were used to compare measured gamma-ray decay energies at a number of cooling times with calculations using ENDF/B-IV[48] and ENDF/B-V[49] fission-product decay data. The method used in the comparison was to rebin the experimental data into wider gamma-energy bins and reduce these to "equivalent pulse data" for each energy bin. These results were then compared with fits to calculated decay gamma-ray spectra generated with CINDER-10[50] and peripheral codes using both the ENDF/B-IV and ENDF/B-V fission-product decay files.

Results of these comparisons shown in Figs. 26-44 indicate that except for very low energies (0.0-0.1 MeV), the ENDF/B-V data do not seem to be any improvement over the ENDF/B-IV data. In fact, for cooling times from about 20 to 200 s, the ENDF/B-V data seem definitely inferior. Both data files, however, are generally deficient, especially for short cooling times (less that 100 s) and high gamma-ray energies (above 800 keV). The results of this study should prove useful in identifying those fission-product nuclides in ENDF/B with deficient decay gamma-ray data. A Los Alamos report describing the details of this work is in preparation.

B. Decay Power Comparisons Using ENDF/B-IV and -V Data in CINDER-10 (T. R. England, W. B.Wilson, R. J. LaBauve, and N. L. Whittemore)

During this reporting period, a number of decay power comparisons using ENDF/B-IV and -V data in CINDER-10 were made. Figures 45-48 compare the pulse and "infinite" cases for ^{235}U and ^{239}Pu. The ANS/ANSI 5.1 (1979) Standard is

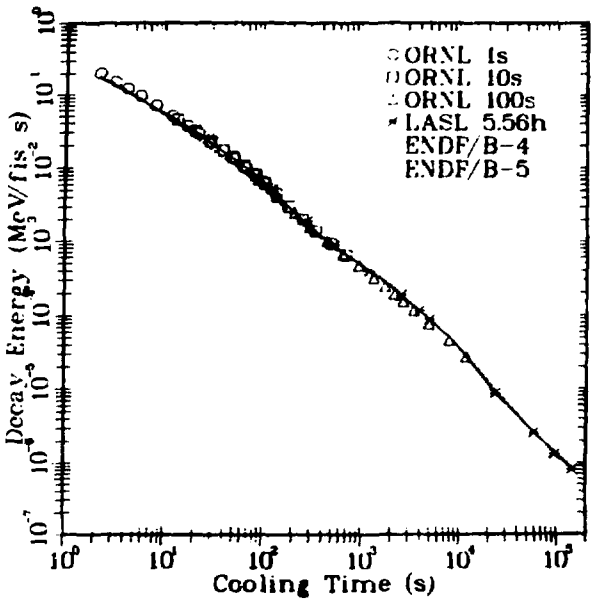

Fig. 26.
Comparison for sum over all groups 0.0-6.0 MeV.

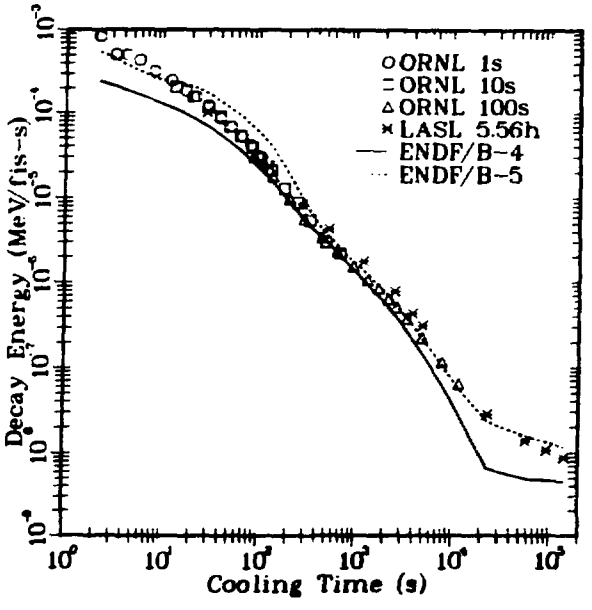

Fig. 27.
Comparison for Group 1 0.0-0.1 MeV.

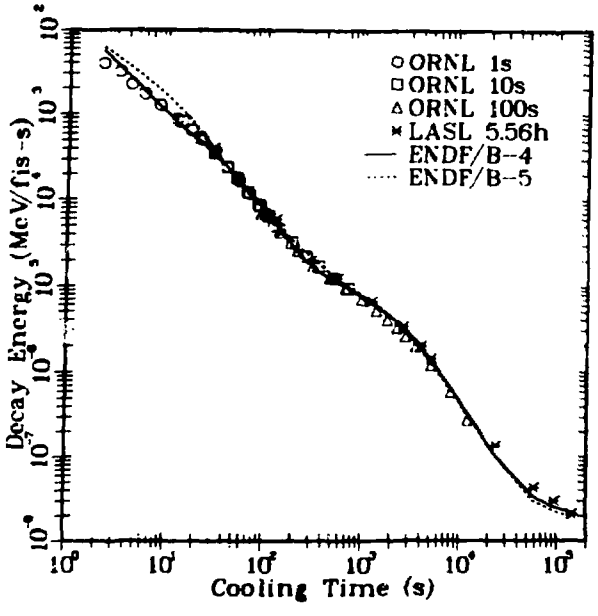

Fig. 28.
Comparison for Group 2 0.1-0.2 MeV.

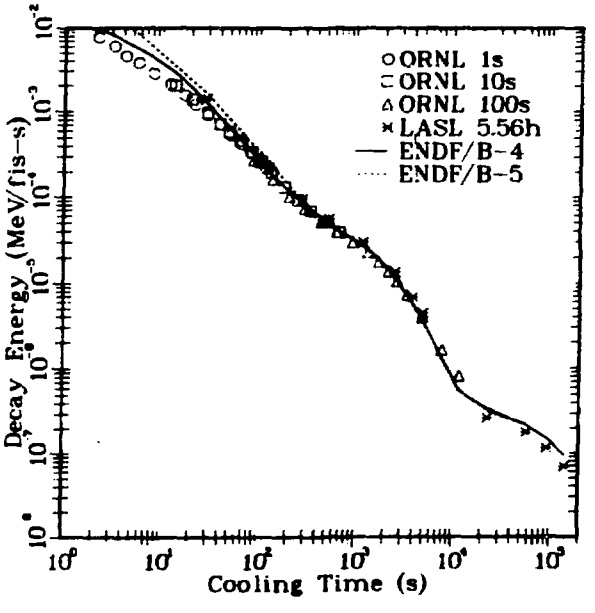

Fig. 29.
Comparison for Group 3 0.2-0.4 MeV.

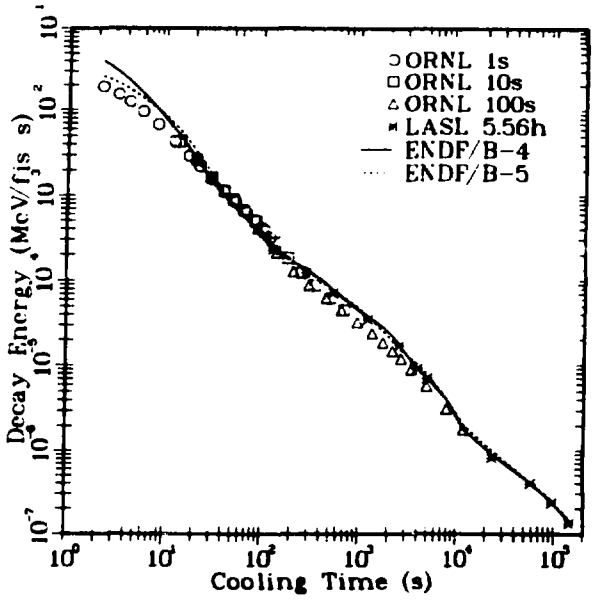

Fig. 30.
Comparison for Group 4 0.4-0.6 MeV.

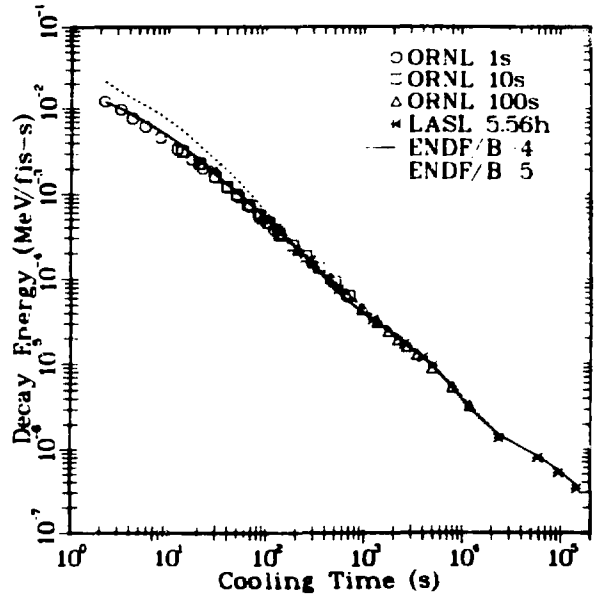

Fig. 31.
Comparison for Group 5 0.6-0.8 MeV.

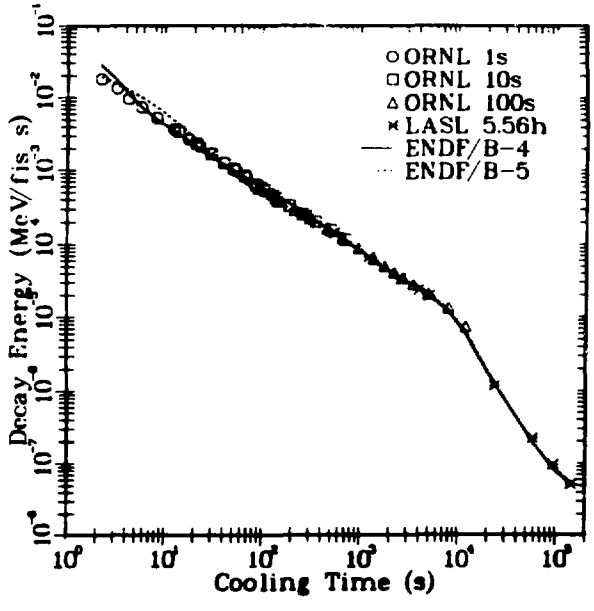

Fig. 32.
Comparison for Group 6 0.8-1.0 MeV.

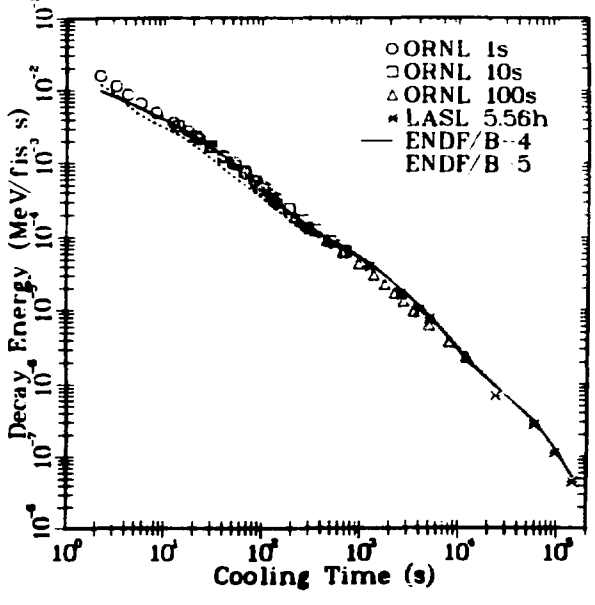

Fig. 33.
Comparison for Group 7 1.0-1.2 MeV.

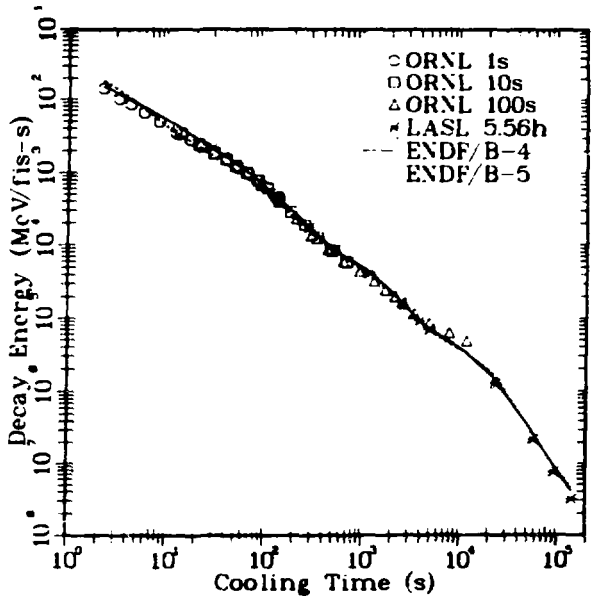

Fig. 34.
Comparison for Group 8 1.2-1.4 MeV.

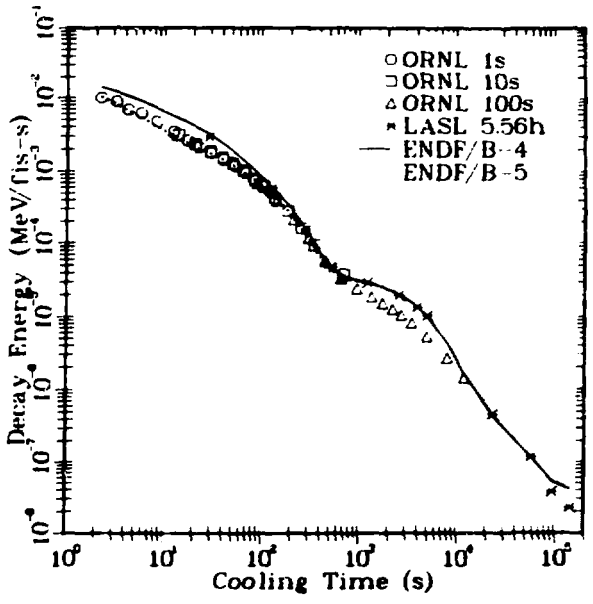

Fig. 35.
Comparison for Group 9 1.4-1.6 MeV.

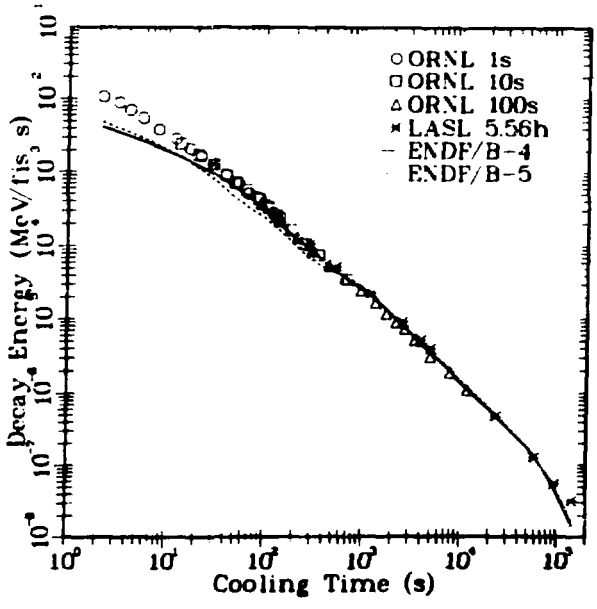

Fig. 36.
Comparison for Group 10 1.6-1.8 MeV.

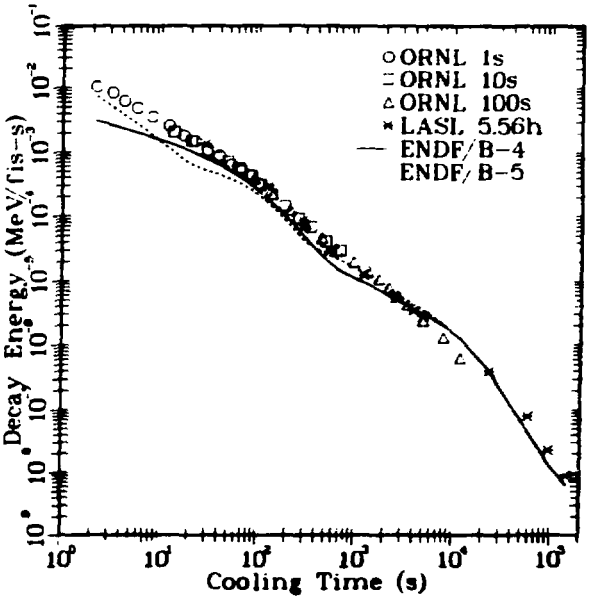

Fig. 37.
Comparison for Group 11 1.8-2.0 MeV.

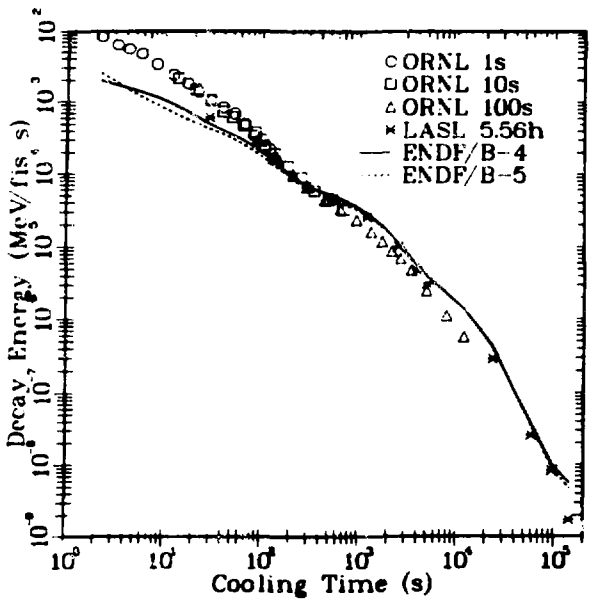

Fig. 38.
Comparison for Group 12 2.0-2.2 MeV.

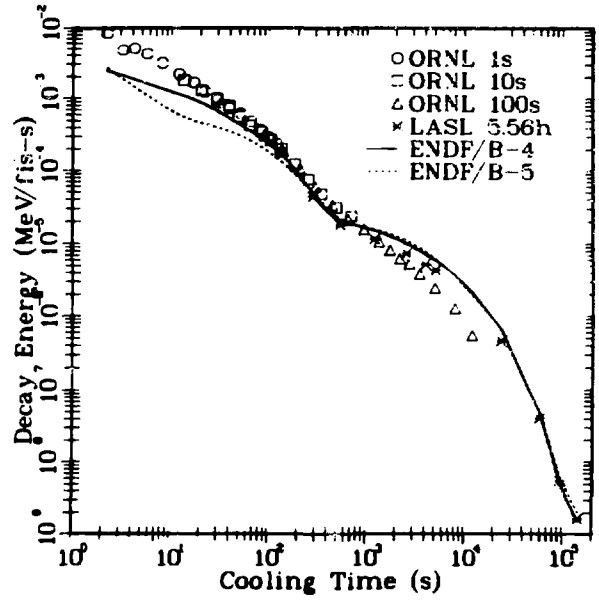

Fig. 39.
Comparison for Group 13 2.2-2.4 MeV.

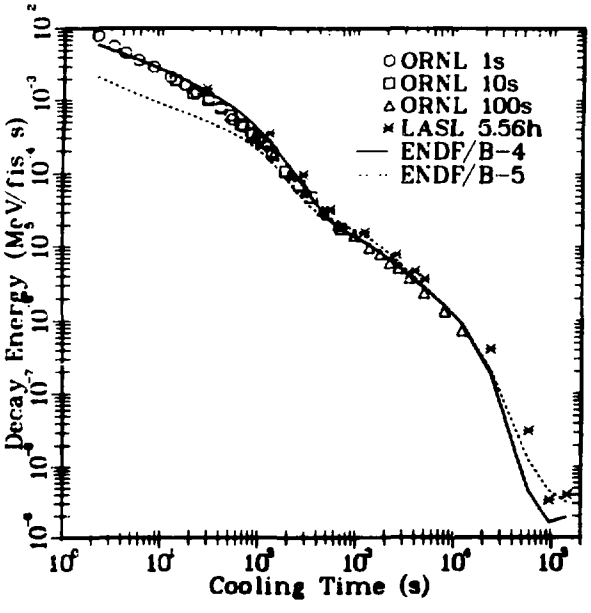

Fig. 40.
Comparison for Group 14 2.4-2.6 MeV.

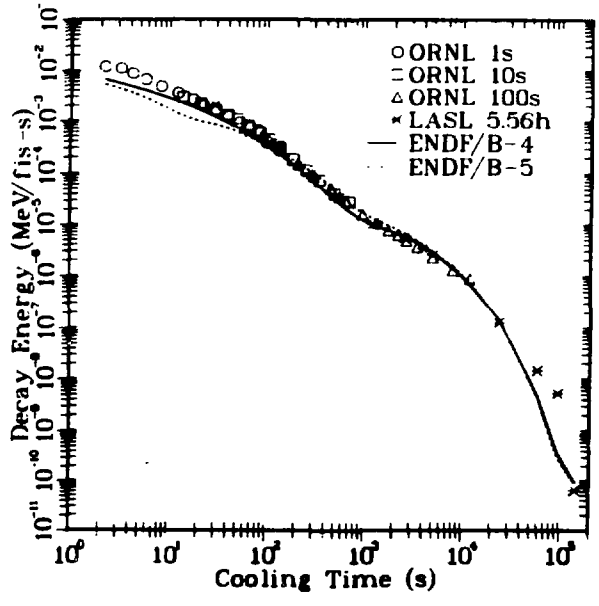

Fig. 41.
Comparison for Group 15 2.6-3.0 MeV.

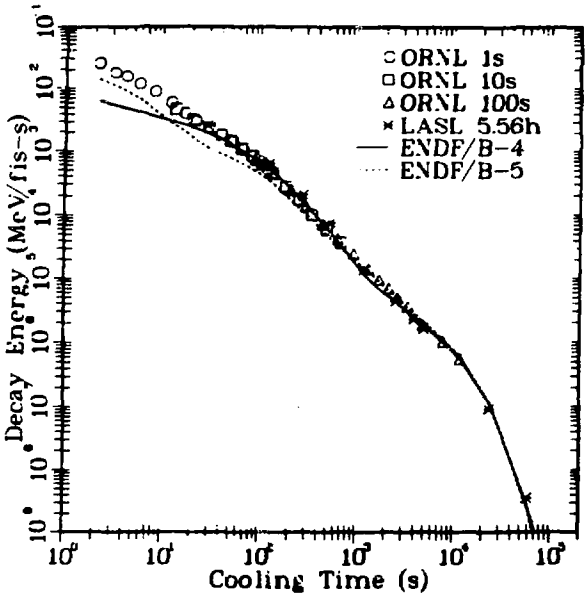

Fig. 42.
Comparison for Group 16 3.0-4.0 MeV.

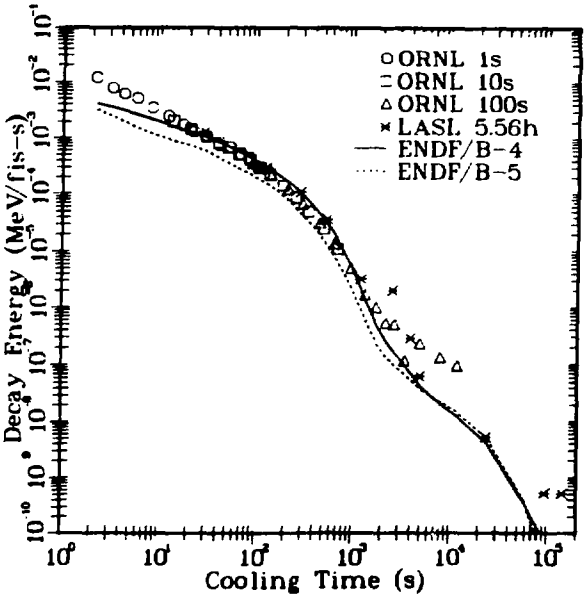

Fig. 43.
Comparison for Group 17 4.0-5.0 MeV.

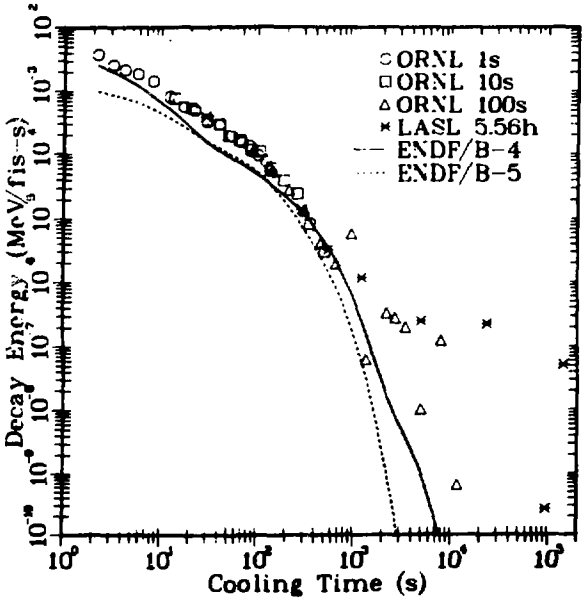

Fig. 44.
Comparison for Group 18 5.0-6.0 MeV.

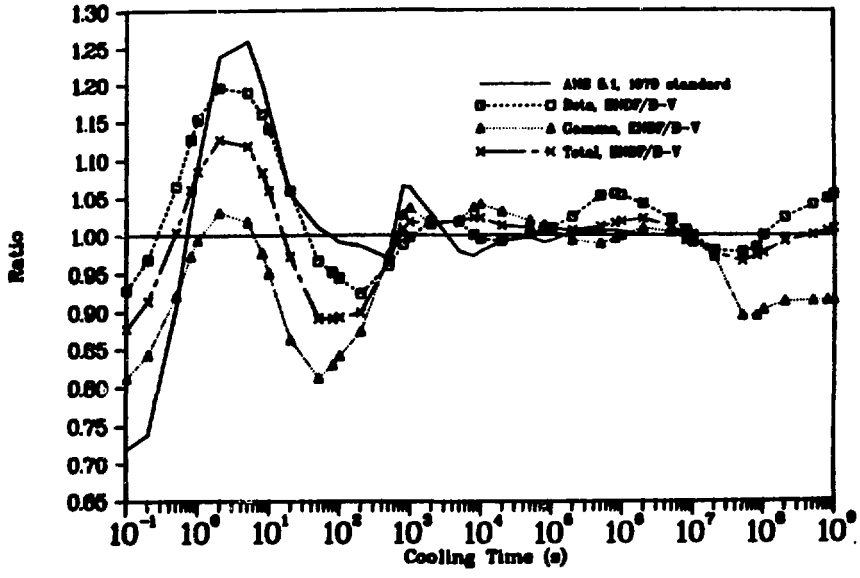

Fig. 45
^{235}U thermal fission pulse comparison of ANS 5.1 and calculated ENDF/B-V fission-product decay powers as a ratio to ENDF/B-IV.

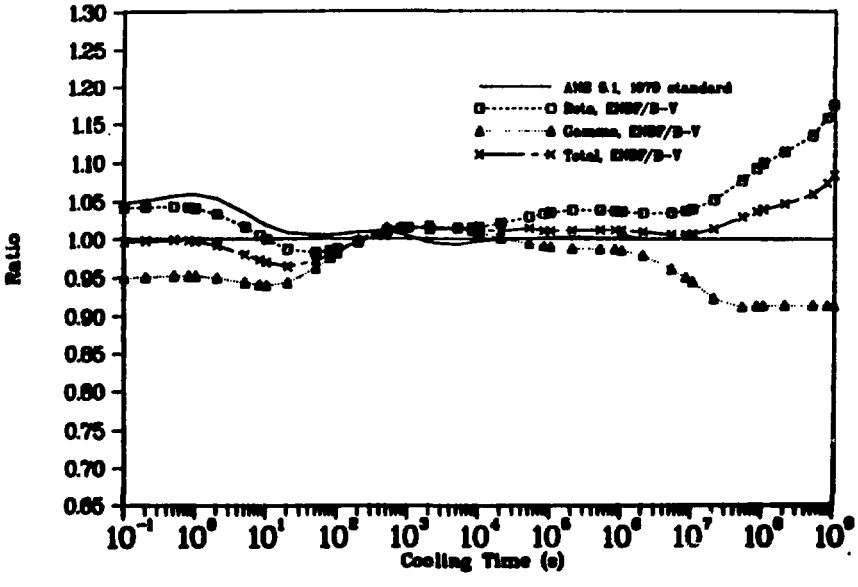

Fig. 46.
^{235}U thermal fission infinite comparison of ANS 5.1 and calculated ENDF/B-V fission-product decay powers as a ratio to ENDF/B-IV, 10^{13} s irradiation, no absorption.

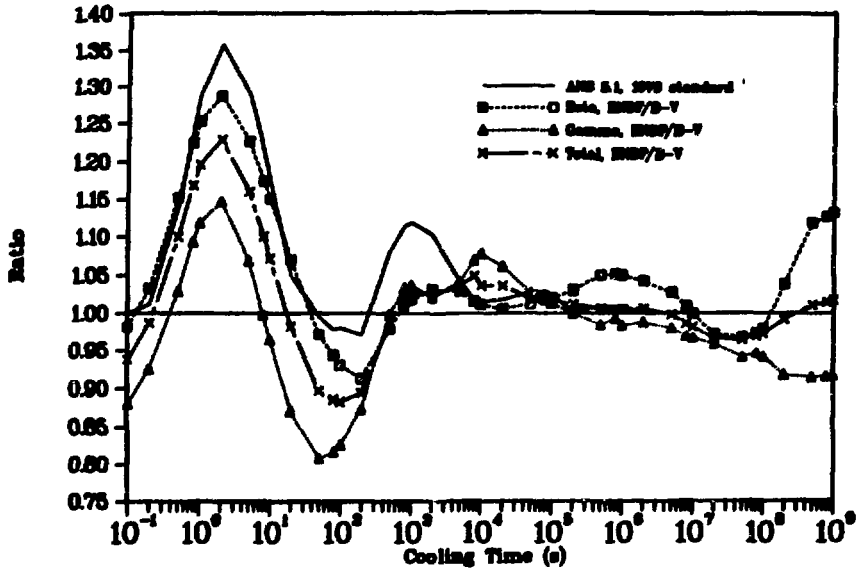

Fig. 47.
^{239}Pu thermal fission pulse comparison of ANS 5.1 and calculated ENDF/B-V fission-product decay powers as a ratio to ENDF/B-IV.

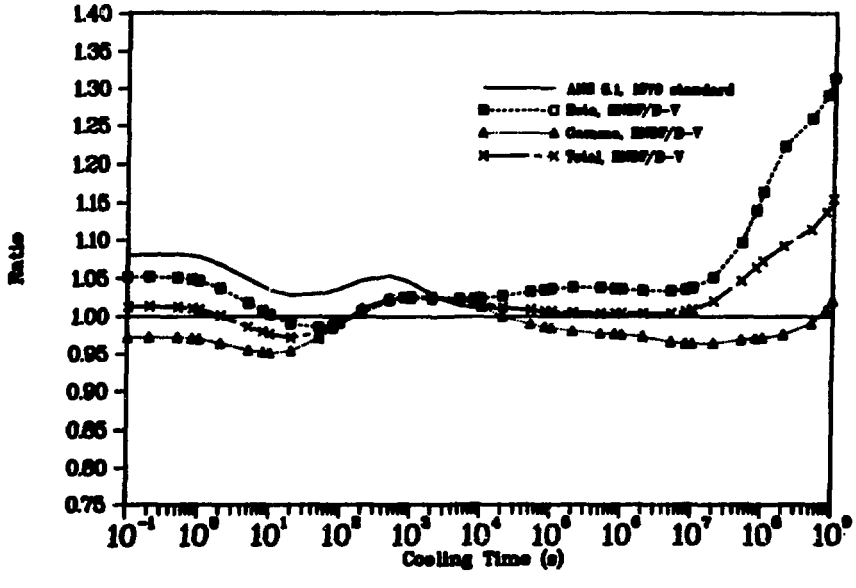

Fig. 48.
^{239}Pu thermal fission infinite comparison of ANS 5.1 and calculated ENDF/B-V fission-product decay powers as a ratio to ENDF/B-IV, 10^{13} s irradiation, no absorption.

included. All of these comparisons are ratios to the calculations using ENDF/B-IV data as listed in LA-6116-MS. The first four plots extend from 0.1 s to ≈ 30 yr.

Figures 49-53 compare the Los Alamos experimental values [as listed in LA-NUREG-6713-MS for ^{235}U and in LA-7452-MS (NUREG/CR-0349) for ^{233}U and ^{239}Pu] as ratios to the calculated values using ENDF/B-IV and -V for each fuel. Figures 54 and 55 compare the ^{239}Pu and ^{233}U total heat rates to ^{235}U for the same 20 000 s irradiation used in the Los Alamos experiment; data on these two figures are calculated, not experimental.

It appears that the shape, and at times the magnitude, of the decay power curve calculated with ENDF/B-V data is in better agreement with the ANS Standard than is that calculated with Version IV. However the first four plots, along with other data, indicate that the calculated gamma decay power component is generally too small and the beta component too large, especially at short cooling times. We are still examining the new ENDF/B-V files in detail. The few errors found to date do not affect the aggregate heating. We reached the following conclusions regarding the calculations for aggregate heating.

- We are confident that the CINDER-10 files are correct and now have an independent confirmation from the Hanford Engineering Development Laboratory using their RIBD code that this is so; that is, we have no significant errors in the processed ENDF/B-V data and CINDER-10 chain structures.

- We have already eliminated the fission yields as a reason for significant differences; the use of ENDF/B-IV decay files with ENDF/B-V yields actually showed a slightly better agreement with the Los Alamos experiment (≈ 1%) than use of only ENDF/B-IV data.

- Calculations for the ^{235}U pulse by Tobias using the United Kingdom (UK) data (UKFPDD-2) and by Yoshida using the October 1980 Japanese file (before their use of only theoretical decay energies for fission products having large Q values) are very similar to ours using ENDF/B-V; Yoshida's calculations for the pulse case are nearly identical to ours.

Therefore, we are confident that any remaining errors are in the basic decay data files and there may well be a deficiency in the experimental spectra for individual nuclides having large Q values, as recently suggested by Yoshida.

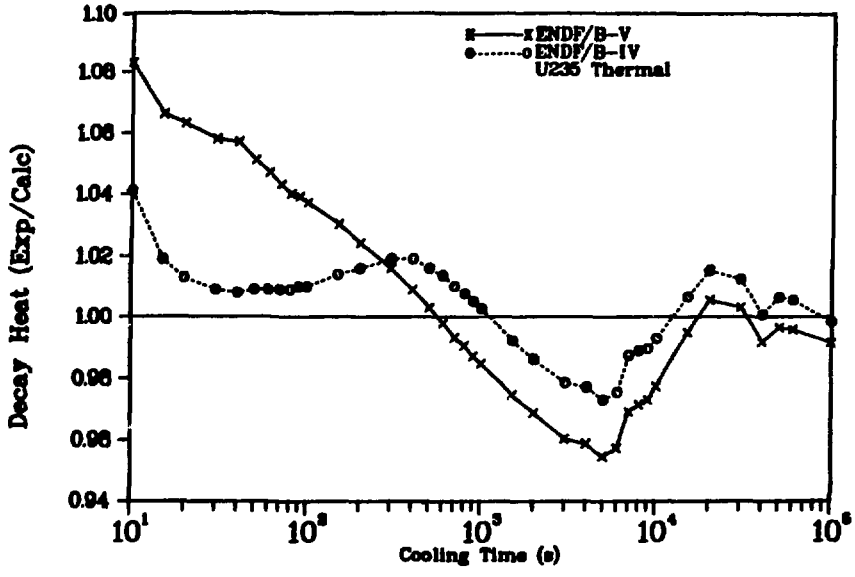

Fig. 49.
Ratio of experimental to calculated decay heat for a 2×10^4 s irradiation at constant flux.

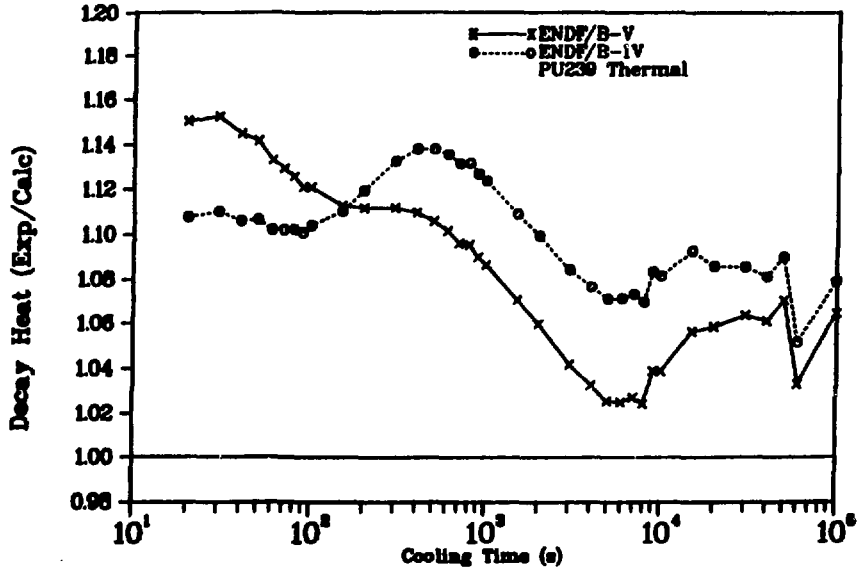

Fig. 50.
Ratio of experimental to calculated decay heat for a 2×10^4 s irradiation at constant flux.

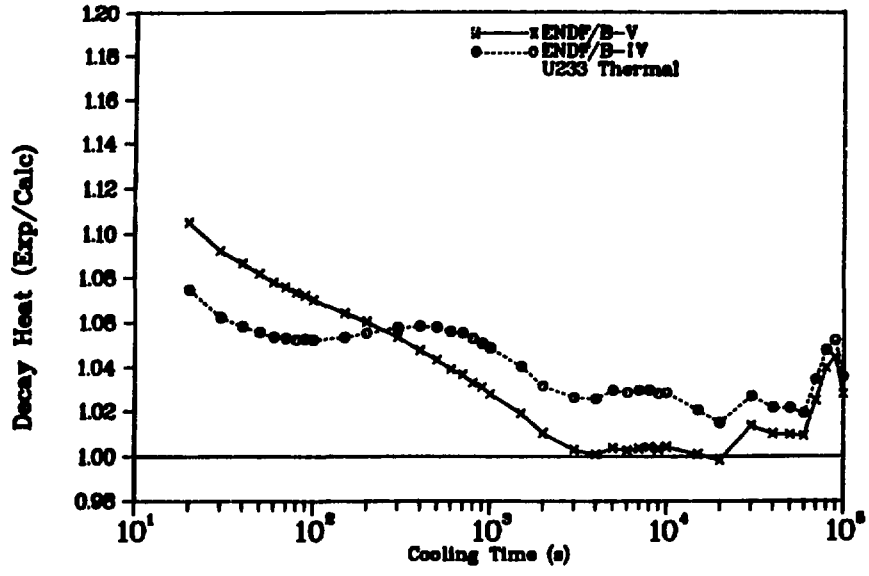

Fig. 51.
Ratio of experimental to calculated decay heat for a 2×10^4 s irradiation at constant flux.

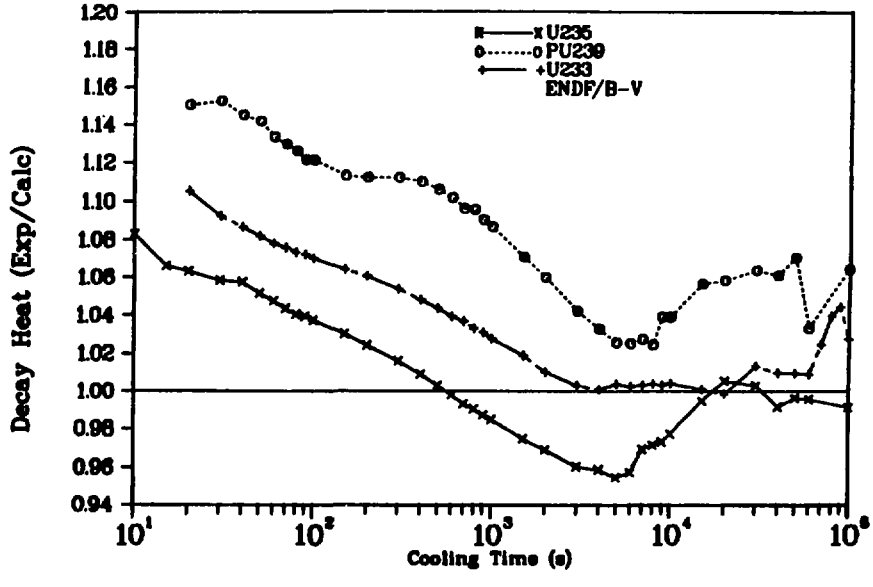

Fig. 52.
Ratio of experimental to calculated decay heat for a 2×10^4 s irradiation at constant flux.

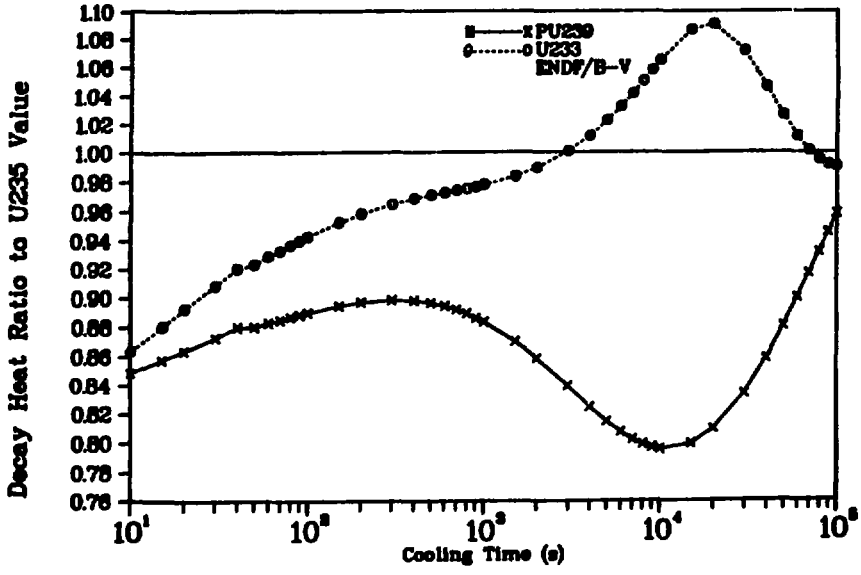

Fig. 53.
Ratio of experimental to calculated decay heat for a 2×10^4 s irradiation at constant flux.

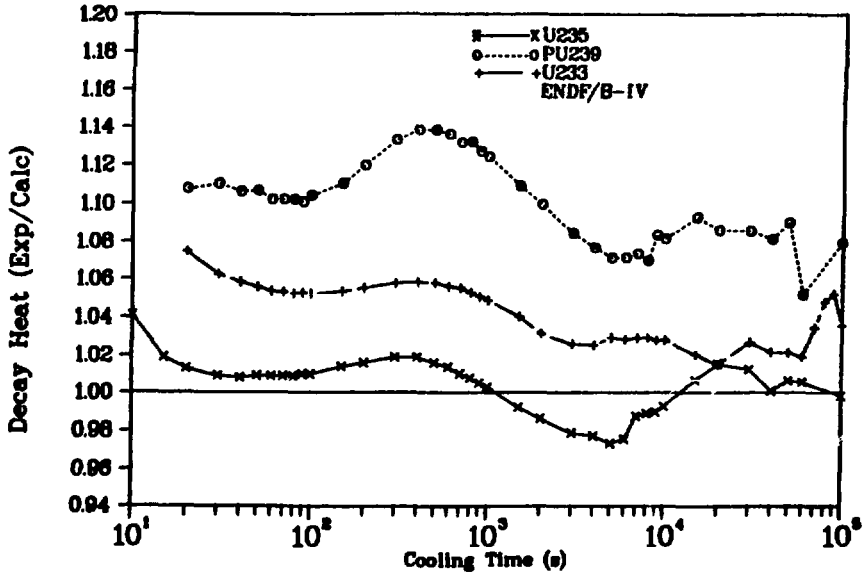

Fig. 54.
Ratio of experimental to calculated decay heat for a 2×10^4 s irradiation at constant flux.

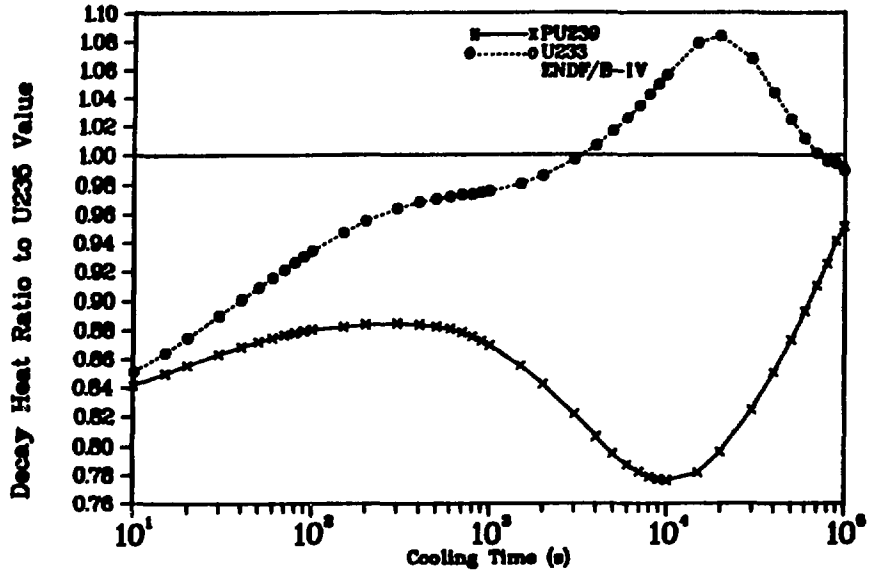

Fig. 55.
Ratio of experimental to calculated ^{239}Pu and ^{233}U and ^{235}U decay heat for 2×10^4 s irradiation at constant flux.

C. ENDF/B-V Data Testing and Summary Data [T. R. England, W. B. Wilson, R. J. LaBauve, and R. E. Schenter (HEDL)]

Apart from decay heat and spectra, processed few-group cross sections, σ_{2200}, and resonance integrals derived from ENDF/B-V have been compared with similar data from ENDF/B-IV and cross sections processed at HEDL. Part of this work is for use in an invited paper for the Miami American Nuclear Society Meeting. An error in the ^{105}Rh cross-section file was found; this nuclide is an important absorber in both LWRs and LMFBRs. Some cross sections show large changes from ENDF/B-IV values, but these are not likely to have a large effect on the aggregate absorption buildup in LWRs. (The effect on LWBRs, evaluated at HEDL, is ≈ 10% increase in the macroscopic absorption.)

A joint Los Alamos/HEDL report containing summary decay parameters and reference cross-section data for actinides and fission products is being prepared. This report will also contain a summary of known errors in the ENDF/B-V data base as detected in data testing at Los Alamos and Hanford and contributed by Tobias (United Kingdom). Other results from data testing are being prepared for the Brookhaven National Data Testing report.

D. SPEC5: Code to Produce Multigroup Spectra (T. R. England, R. J. LaBauve, W. B. Wilson and N. L. Whittemore)

This code produces multigroup spectra for gamma plus x-ray, $\beta^{\pm}$, α, anti-neutrino, and neutrino radiations from ENDF/B-V input. A modification for low β^{-} end-point energies was made, and all spectra were computed for the unstable fission products having an evaluated spectra (265 of the 750 unstable products) and for all 60 actinides in ENDF/B-V. These multigroup spectra include net particles and energies in energy bins of 10 keV up to 100 keV, followed by 50-keV bins through 7.5 MeV--a total of 158 groups. The gamma spectra were augmented and collapsed to few groups and used in comparison studies described in Sec. III-A. Otherwise the SPEC5 code is still under development, primarily to generate beta and antineutrino spectra for nuclides having no measured end-point energies. A routine to broaden the gamma lines must also be added.

E. Calculation of H. B. Robinson-2 Fuel Isotopics and Comparison with Measurements [W. B. Wilson, R. J. LaBauve, T. R. England, G. E. Bosler (Q-1), and J. R. Phillips (Q-1)]

The H. B. Robinson-2 reactor (HBR2) is a conventional 3-zone, 2200 MW PWR designed by Babcock and Wilcox and operated since 1971 at Hartsville, SC by the Carolina Power & Light Co. HBR2 assembly B05 was irradiated in HBR2 cycles 1 and 2 and discharged in 1974 with an assembly-averaged exposure of approximately 28 000 MWd/t. Because of the documented power history[51] and existence of radionuclide inventory measurements[52,53] for fuel samples of the assembly, the HBR2 B05 fuel has served widely as a benchmark for isotopics calculations and is specified for testing calculations with the Electric Power Research Institute (EPRI) fuel-cycle codes.[54] In performing a range of HBR2 actinide nuclide inventory parameter sensitivity studies with tandem EPRI-CELL/CINDER-2 calculations, we have first calculated fuel properties for comparison with the available measured data.

Three fuel samples of HBR2 B05 Rod P8 were destructively analyzed by Battelle Columbus Lab in 1975 following 1.4 yr cooling. The burnup (atom % fission) of each sample was determined using ASTM method E321-69[55] for burnup analyses by mass-spectrometic neodymium-148 determination, and a variety of uranium and plutonium isotopic ratios were measured. One of the samples was taken from the fuel in a grid spacer region and was rejected as a refrence because of the atypical flux spectrum there. Tandem EPRI-CELL/CINDER-2 calculations were made for the two remaining P8 samples.

EPRI-CELL calculations used the ENDF/B-V based nuclear-data library and the appropriate enrichment, density, and temperature of the fuel to follow the depletion and buildup of fissionable nuclides through the 34 time intervals used to describe the power history of the assembly. Flux values and nuclide density dependent fission and (n,γ) cross sections for $^{234,235,236,238}U$ and $^{239-242}Pu$ were computed at the beginning of each time interval at four radial points in the fuel rod and recorded on a file for the subsequent CINDER-2 calculation.

CINDER-2 repeated the recorded power history using the cross sections and fluxes averaged over the fuel at each interval to calculate the average inventory across the fuel. The complete cycle of calculations was repeated until calculated burnup (atom % fission) agreed with that reported for the measured samples. CINDER-2 followed the production, transmutation, and decay of 186 fission-product and 46 actinide nuclides throughout the power history and 1.4-yr decay period of the samples. The resulting calculated inventory values were used to form the nuclide ratio quantities used in reporting the P8 measurement. Calculated and measured values are compared in Table VII, where measured and calculated values agree within ± 15%. The largest differences occurred between measured and calculated ^{234}U and ^{238}Pu values; these nuclides are produced both by (n,2n) reactions and by ^{242}Cm decay, and the disagreements may indicate uncertainties in nuclear data parameters used in calculating the inventory of the nuclides. No uncertainties are given for the measured P8 values.

Samples taken from Rod E14 of the same assembly have been examined by group CNC-11 at Los Alamos. The inventory of 8 fission-product nuclides and 14 actinide nuclides was measured for 1 sample after 4.86 yr cooling, but the burnup of the sample is unknown. The results of the E14 measurements are compared in Table VIII with the equivalent quantities computed for the P8 samples calculated for the longer cooling time. The high measured concentrations of ^{238}U and ^{239}Pu indicate a small normalization problem between measurement and calculation. As in the comparison with the P8 sample measurements, ^{234}U and ^{238}Pu concentrations appear to be undercalculated. Most significant is the agreement of higher actinide nuclide densities.

Reports describing these HBR2 fuel inventory comparisons and higher actinide production-sensitivity studies are in preparation.

TABLE VII

COMPARISON OF MEASURED AND CALCULATED H. B. ROBINSON-2 ISOTOPIC RATIOS[a]

Quantity	Sample P8A			Sample P8B		
	Measured Value	Calc. Value	% Difference	Measured Value	Calc. Value	% Difference
Burnup, Atom % fission	2.559	2.560	+ 0.04	3.221	3.221	+ 0.01
Exposure Mwd/T	24570	24660	+ 0.37	30920	31191	+ 0.89
U-234/U	0.00016	0.00014	-14.04	0.00014	0.00012	-12.81
U-235/U	0.00816	0.00828	+ 1.53	0.00612	0.00588	- 3.84
U-236/U	0.00326	0.00322	- 1.08	0.00352	0.00357	+ 1.52
U/238/U	0.98842	0.98835	- 0.01	0.99022	0.99043	+ 0.02
Pu-238/Pu	0.01143	0.00979	-14.35	0.01676	0.01452	-13.35
Pu-239/Pu	0.59557	0.59365	- 0.32	0.54261	0.53966	- 0.54
Pu-240/Pu	0.23290	0.22766	- 2.25	0.25101	0.24002	- 4.38
Pu-241/Pu	0.11842	0.12385	+ 4.58	0.12998	0.13772	+ 5.95
Pu-242/Pu	0.04168	0.04506	+ 8.10	0.05964	0.06807	+11.41
Pu-239/U-238	0.00494	0.00486	- 1.61	0.00518	0.00496	- 4.28
Nd-148/U-238	0.000450	0.000467	+ 3.74	0.000570	0.000593	+ 3.96

[a]Measured isotopic ratios reported in Battelle Columbus Laboratories report BMI-1938, p.16, (1975). Calculated values from 3/81 tandem CELL/CINDER-2 calculations using a detailed power history and 506.75-day cooling.

TABLE VIII

COMPARISON OF H. B. ROBINSON-2 ASSEMBLY B05 SPENT FUEL ISOTOPICS

(Measurements by Los Alamos/CNC-11 of Rod E14 sample; calculations by Los Alamos/T-2 of Rod P8 samples)

Quantity	Measured[a] Rod E14 Sample	EPRI-CELL/CINDER-2 Calculation[b] Rod P8 Sample A	Rod P8 Sample B
Atom % Fission	----------	2.560	3.221
MWd/t	----------	24660	31191
Nuclide densities, atoms/gm oxide at 4.86 yr cooling			
^{90}Sr	2.73 + 18	2.092 + 18	2.493 + 18 c
^{106}Ru	>1.71 + 16	2.018 + 16	2.866 + 16
^{125}Sb	7.45 + 15	7.365 + 15	9.825 + 15
^{134}Cs	7.61 + 16	5.034 + 16	7.943 + 16
^{137}Cs	3.75 + 18	3.116 + 18	3.935 + 18
^{144}Ce	1.41 + 16	1.210 + 16	1.486 + 16
^{154}Eu	3.92 + 16	5.638 + 16	8.741 + 16 c
^{155}Eu	1.28 + 16	1.518 + 16	2.301 + 16 c
^{234}U	3.24 + 17	2.941 + 17	2.603 + 17 c
^{235}U	1.34 + 19	1.759 + 19	1.239 + 19
^{236}U	7.68 + 18	6.845 + 18	7.497 + 18 c
^{238}U	2.15 + 21	2.098 + 21	2.086 + 21 c
^{237}Np	8.19 + 17	6.278 + 17	8.335 + 17
^{238}Pu	3.25 + 17	1.659 + 17	2.744 + 17 c
^{239}Pu	1.08 + 19	1.020 + 19	1.034 + 19 c
^{240}Pu	5.23 + 18	3.909 + 18	4.778 + 18 c
^{241}Pu	2.18 + 18	1.806 + 18	2.241 + 18
^{242}Pu	1.29 + 18	7.739 + 17	1.304 + 18
^{241}Am	6.55 + 17	5.382 + 17	6.589 + 17
^{243}Am	2.2 + 17 ±20%	1.193 + 17	2.623 + 17
^{242}Cm	1.8 + 13	1.306 + 13	1.982 + 13
^{244}Cm	5.10 + 16 ±20%	1.960 + 16	5.900 + 16

[a] Experimental uncertainty ± 5% unless otherwise indicated.

[b] [atoms/g] from calculated [atoms/cm^3]/9.95 g/cm^3.

[c] Measured value outside of range of calculated values.

REFERENCES

1. G. M. Hale and H. Zankel, "Coulomb Corrections in the Three Nucleon System," in "Applied Nuclear Data Research and Development October 1 - December 31, 1980," Los Alamos Scientific Laboratory report LA-8757-PR, p. 1 (1981).

2. Y. H. Chiu and F. W. F. Firk, "Studies of n-^{6}Li Scattering and the Structure of ^{7}Li," 5th International Symposium, Santa Fe, New Mexico, August 1980, in Polarization Phenomena in Nuclear Physics-1980, G. G. Ohlsen, R. E. Brown, N. Jarmie, N. W. McNaughton, and G. M. Hale, Eds., (American Institute of Physics, New York, 1981) No. 69 p. 1311.

3. N. Jarmie, F. D. Correll, R. E. Brown, R. A. Hardekopf, and G. M. Hale, "A New Level in ^{7}Li," Bull. Am. Phys. Soc. 26, 565 (1981).

4. D. M. Hetrick and C. Y. Fu, "GLUCS: A Generalized Least-Squares Program for Updating /Cross-Section Evaluations with Correllated Data Sets," Oak Ridge National Laboratory report ORNL/TM-7341 (ENDF-303) (1980).

5. D. R. Harris, W. A. Reupke, and W. B. Wilson, "Consistency Among Differential Nuclear Data and Integral Observations: The ALVIN Code for Data Adjustment, Sensitivity Calculations, and for Identification of Inconsistent Data," Los Alamos Scientific Laboratory report LA-5987 (1975).

6. D. E. Cullen, K. L. Hill, R. J. Howerton, and S. T. Perkins, "ECSIL: A System for Storage, Retrieval, and Display of Experimental Neutron Data," Lawrence Livermore Laboratory report UCRL-50400, Vol. 1, Rev. 3 (1976).

7. H. H. Hogue, P. L. von Behren, D. W. Glasgow, S. G. Glendinning, P. W. Lisowski, C. E. Nelson, F. O. Purser, and W. Mornow, "Elastic and Inelastic Scattering of 7- to 14-MeV Neutrons from Lithium-6 and Lithium-7," Nucl. Sci. Eng. 69, 22 (1979).

8. O. Bersillon, Bruyeres-le-Chatel, France, personal communication to E. Arthur (1980).

9. D. L. Smith, M. M. Bretscher, and J. W. Meadows, "Measurement of the Cross Section for the ^{7}Li(n,n't)^{4}He Reaction in the Energy Range 7-9 MeV," personal communication (1980).

10. M. T. Swinhoe and C. A. Uttley, "Tritium Breeding in Fusion," Proc. Conf. on Nuclear Cross Sections for Technology, Knoxville, Tennessee, October 22-26 1979, National Bureau of Standards Special Publication 594, 246 (1980).

11. E. D. Arthur, "Calculation of Neutron Cross Sections on Isotopes of Yttrium and Zirconium," Los Alamos Scientific Laboratory report LA-7789-MS (1979).

12. R. C. Haight, S. M.Grimes, R. G. Johnson, and H. H. Barschall, "Charged-Particle Emission in Reactions of 15-MeV Neutrons with ^{89}Y, ^{90}Zr, and ^{92,94,95,96}Mo," Phys. Rev. C 23, 700 (1981).

13. Ch. Lagrange, "Optical Model Calculations of Nucleon Interactions with ^{93}Nb from 10 keV up to 50 MeV," Proc. Int. Conf. on Nucl. Cross Sections for Technology 594, 311 (1980).

14. Ch. Lagrange, "Coherent Optical and Statistical Model Calculations of Neutron Cross Sections for Even A Mo Isotopes," 2nd Advisory Group Meeting on Fission Product Nuclear Data, Petten, the Netherlands (1977).

15. C. H. Johnson, A. Galonsky, and C. N. Inskeep, "Cross Sections for (p,n) Reactions in Intermediate Weight Nuclei," Oak Ridge National Laboratory report ORNL 2910, p. 25 (1960).

16. Y. Yeivin, J. H. Marable, C. R. Weisbin, and J. J. Wagschal, "ORACLE: An Adjusted Cross-Section and Covariance Library for Fast-Reactor Analysis," Proc. 1980 Advances in Reactor Physics and Shielding Conference, Sun Valley, Idaho, p. 705 (1981).

17. A. Prince, M. K. Drake, and P. Hlavac, "An Analysis of the ^{239}Pu Neutron Cross Sections from 20 keV to 20 MeV," Brookhaven National Laboratory report BNL-50388 (1973).

18. J. Raynal, "Optical Model and Coupled-Channel Calculations in Nuclear Physics," International Atomic Energy Agency report IAEA-SMR-9/8 (1972).

19. G. Haout, Ch. Lagrange, J. Lachkar, J. Jary, Y. Patin, and J. Sigaud, "Fast Neutron Cross Sections for Actinide Nuclei," Proc. Int. Conf. on Nuclear Cross Sections for Technology, National Bureau of Standards Special Publication 594, 672 (1980).

20. W. P. Poenitz, J. F. Whalen, and A. B. Smith, "Total-Neutron Cross Sections of Heavy Nuclei," Proc. Int. Conf. on Nucl. Cross Sections for Technology, National Bureau of Standards Special Publication 594, 698 (1980).

21. Taro Tamura, "Computer Program JUPITOR-1 for Coupled-Channel Calculations," Oak Ridge National Laboratory report ORNL-4152 (August 1967).

22. Taro Tamura, U. of Texas, Austin, private communication (January 1981).

23. D. G. Madland and J. R. Nix, "Calculation of Prompt Fission Neutron Spectra," Trans. Am. Nucl. Soc. 32, 726 (1979).

24. D. G. Madland and J. R. Nix, "Calculation of Prompt Fission Neutron Spectra," Bull. Am. Phys. Soc. 24, 885 (1979).

25. D. G. Madland and J. R. Nix, "Calculation of Prompt Fission Neutron Spectra," Proc. Int. Conf. on Nuclear Cross Sections for Technology, Knoxville, Tennessee, October 22-26, 1979, National Bureau of Standards Special Publication 594, p. 788 (1980).

26. D. G. Madland and J. R. Nix, "Calculation of Neutron Spectra and Average Neutron Multiplicities from Fission," Proc. Int. Conf. on Nuclear Physics, Berkeley, California, August 24-30, 1980 (to be published).

27. D. G. Madland, "Prompt Fission Neutron Spectra and $\bar{\nu}_p$," Proc. Workshop on Evaluation Methods and Procedures, Brookhaven National Laboratory, September 22-25, 1980 (to be published).

28. M. Abramowitz and I. A. Stegun, Eds., Handbook of Mathematical Functions (National Bureau of Standards, Washington, D.C., 1964) pp. 227-266.

29. J. P. Unik, J. F. Gindler, L. E. Glendenin, K. F. Flynn, A. Gorski, and R. K. Sjoblom, "Fragment Mass and Kinetic Energy Distributions for Fissioning Systems Ranging from Mass 230 to 256," Proc. Third IAEA Symp. on Physics and Chemistry of Fission, Rochester, New York, 1973, Vol. II, p. 19 (1974).

30. A. H. Wapstra and K. Bos, "The 1977 Atomic Mass Evaluation," Atomic Data Nuclear Tables 19, 177 (1977).

31. W. D. Myers, Droplet Model of Atomic Nuclei (IFI/Plenum Data Co., New York 1977).

32. D. C. Hoffman and M. M. Hoffman, "Post-Fission Phenomena," Annu. Rev. Nucl. Sci. 24, 151 (1974).

33. R. Kinsey, Ed., Data Formats and Procedures for the Evaluated Nuclear Data File, ENDF (National Nuclear Data Center, Brookhaven National Laboratory, Upton, New York, 1979) p. 5.4.

34. J. W. Boldeman, D. Culley, and R. J. Cawley, "The Fission Neutron Spectrum from the Spontaneous Fission of ^{252}Cf," Trans. Am. Nucl. Soc. 32, 733 (1979).

35. F. D. Becchetti and G. W. Greenlees, "Nucleon-Nucleus Optical Model Parameters, A>40, E<50 MeV," Phys. Rev. 182, 1190 (1969).

36. J. R. Smith, "Status of ^{252}Cf ν and Its Impact on Thermal Reactor Parameters," Proc. Symp. on Nuclear Data Problems for Thermal Reactor Applications, May 22-24, 1979, Upton, New York, Electric Power Research Institute report EPRI NP-1093 p. 5-1 (1979).

37. R. E. MacFarlane, "Energy Balance of ENDF/B-V," Trans. Am. Nucl. Soc. 33, 681 (November 1979).

38. T. A. Gabriel, J. D. Amburgey, and N. M. Greene, "Radiation Damage Calculations: Primary Knock-On Atom Spectra, Displacement Rates, and Gas Production Rates," Nucl. Sci. Eng. 62, 21 (1976).

39. R. Protsik, E. Kujawaski, and C. L. Cowan, "TDOWN-IV: A Computer Code to Generate Composition and Spatially Dependent Neutron Cross Sections for Multigroup Neutronics Analysis," General Electric Company report GEFR-00485 (September 1979).

40. R. Douglas O'Dell, Forest W. Brinkley, Jr., and Duane R. Marr, "Users' Manual for ONEDANT: A Code Package for One-Dimensional Diffusion-Accelerated, Neutron-Particle Transport," personal communication.

41. ENDF/B-V data for ^{2}H (MAT 1302), evaluation by L. Stewart (Los Alamos) and A. Horsely (AWRE); and the ENDF/B-V data file for ^{16}O (MAT 1276), evaluation by P. G. Young, D. G. Foster, and G. M. Hale, Los Alamos; in the Brookhaven National Laboratory report BNL-NCS-17541 (ENDF-201) available from the National Nuclear Data Center at Brookhaven (July 1979).

42. R. E. MacFarlane, R. J. Barrett, D. W. Muir, and R. M. Boicourt, "The NJOY Nuclear Data Processing System: User's Manual," Los Alamos Scientific Laboratory report LA-7584-M (1978).

43. R. C. Weast, Ed., Handbook of Chemistry and Physics, 55th Edition (CRC Press, Cleveland, Ohio, 1974).

44. C. E. Eisenhauer, National Bureau of Standards, personal communication.

45. P. Moller and J. R. Nix, "Nuclear Mass Formula with a Yukawa-Plus-Exponential Macroscopic Model and a Folded-Yukawa Single-Particle Potential," in Nucl. Phys. A361, No. 1, pp. 117-146 (May 18, 1981).

46. J. K. Dickens, T. A. Love, J. W. McConnell, J. F. Emery, K. J. Northcutt, R. W. Peelle, and H. Weaver, "Delayed Beta- and Gamma-Ray Production Due to Thermal-Neutron Fission of ^{235}U, Spectral Distributions for Times After Fission Between 2 and 14 000 sec: Tabular and Graphical Data," Oak Ridge National Laboratory report NUREG/CR-0162, ORNL/NUREG-39 (August 1978).

47. E. T. Jurney, P. J. Bendt, and T. R. England, "Fission Product Gamma Spectra," Los Alamos Scientific Laboratory report LA-7620-MS (January 1979).

48. Fission-Product Decay Library of the Evaluated Nuclear Data File, Version IV (ENDF/B-IV). [Available from and maintained by the National Nuclear Data Center (NNDC) at Brookhaven National Laboratory.]

49. Fission-Product Decay Library of the Evaluated Nuclear Data File, Version V (ENDF/B-V). [Available from and maintained by the National Nuclear Data Center (NNDC) at Brookhaven National Laboratory.]

50. T. R. England, R. Wilczynski, and N. L. Whittemore, "CINDER-7: An Interim Report for Users," Los Alamos Scientific Laboratory report LA-5885-MS (April 1976). [CINDER-10, the version used in this report is unpublished; it is described in "Applied Nuclear Data Research and Development January 1-March 31, 1976," Los Alamos Scientific Laboratory report LA-6472-PR, p. 60 (1976) and in "Applied Nuclear Data Research and Development October 1-December 31, 1975," Los Alamos Scientific Laboratory report LA-6266-PR, p. 13 (1976).]

51. S. J. Dagbjartsson, B. A. Murdock, D. E. Owen, and P. E. MacDonald, "Axial Gas Flow in Irradiated PWR Fuel Rods," Idaho National Engineering Laboratory report TREE-NUREG-1158 (September 1977).

52. A. A. Bauer, L. M. Lowry, and J. S. Perrin, "Progress on Evaluating Strength and Ductility of Irradiated Zircolay During July Through September, 1975," Battelle Columbus Laboratories report BMI-1938 (September 1975).

53. A. E. Norris, Los Alamos National Laboratory, private communication (1981).

54. O. Ozer, Electric Power Research Institute, private communication to W. B. Lohwenstein and B. A. Zolatar (April 6, 1976).

55. 1974 Annual Book of ASTM Standards, Standard Method of Test Atom Percent Fission in Uranium and Plutonium Fuel (Nd-148), E321-69, pp. 721-729